

ENANTIOSELECTIVE SYNTHESIS OF AN ANTICANCER RUTHENIUM POLYPYRIDYL
COMPLEX (RPC) AND INFLUENCE OF CHIRAL SELECTIVITY ON
DNA PHOTOCLEAVAGE

by

Shomita Ferdous

Presented to the Faculty of the Graduate School of
The University of Texas at Arlington in Partial Fulfillment
of the Requirements
for the Degree of

MASTER OF SCIENCE IN CHEMISTRY

THE UNIVERSITY OF TEXAS AT ARLINGTON

December 2017

Copyright © by Shomita Ferdous 2017

All Rights Reserved



Acknowledgements

I would like to express my sincere gratitude to my supervisor Dr. Frederick M. MacDonnell for giving me the chance to work as a graduate student in his research lab. Dr. MacDonnell has been a great mentor who always guided me to the right direction for completing my research and course works successfully. I had the chance to gain in depth knowledge in chemistry from his valuable lectures and research ideas. Being a graduate student in his lab, I gained clarity in theoretical knowledge and skills in research works. He has always inspired me to think independently and scientifically. He has guided me in all the times of my experiments and writing of this thesis. I will always be thankful for the patience, motivation and support I got from him to achieve my Masters degree.

I would also like to give my special thanks to my dissertation committee members Dr. Brad Pierce and Dr. Rasika Dias for their valuable advices throughout my graduate studies. I had the chance to attend their lecture classes and gained a great deal of knowledge which made me more confident to become a good researcher in chemistry.

I also want to acknowledge all my lab members who have helped me achieving my goal in every possible way. I have received immense support and great advice from Dr. Nagham Alatrash for my research and studies. My lab mate Cynthia Griffith has always helped me solving any critical problem or learning new equipment operation. I had valuable and insightful discussions with my lab members Dr. Faiza Issa and Srikanth Reddy Medipelli that helped me to enrich my knowledge and to complete this dissertation.

I am also thankful to all my faculty members, my graduate advisors Dr. Kroll and Dr. Macaluso and my teaching assistantship supervisor Dr. Cleaver who have helped me with all kinds of assistance I needed to complete my education in this university.

Finally, I am thankful to my parents for their endless support and love for me throughout the path of my higher studies. Their faith and love have helped me in every step of my life to come so far.

November 08, 2017

Abstract

ENANTIOSELECTIVE SYNTHESIS OF AN ANTICANCER RUTHENIUM POLYPYRIDYL COMPLEX (RPC) AND INFLUENCE OF CHIRAL SELECTIVITY ON DNA PHOTOCLEAVAGE

Shomita Ferdous, MS

The University of Texas at Arlington, 2017

Supervising Professor: Frederick M. MacDonnell

Ruthenium polypyridyl complexes (RPCs) represent a promising therapeutic class of drugs for transition-metal based anticancer drug development. The complex $[(\text{phen})_2\text{Ru}(\text{tatpp})\text{Ru}(\text{phen})_2]$ (4^{4+}) is a RPC which has shown success in both cell free and cellular assay. Unlike many other RPCs, 4^{4+} can selectively kill malignant cells without light irradiation from external sources. This binuclear complex 4^{4+} is a DNA intercalator containing redox-active ligand tatpp (9,11,20,22-Tetraaza tetrapyrido[3,2-a:2'3'-c:3",2"- 1:2"',3''']-pentacene) which cleaves DNA in presence of a mild reducing agent, i.e. glutathione (GSH).^{1,2,3} The cellular assay (MTT assay) with different types of malignant cells has also established this as an equally potent cytotoxic agent both under normoxic and hypoxic conditions.¹ According to the recent report, the cytotoxicity of 4^{4+} can also be increased by tuning the polypyridyl ligands and making them more lipophilic (IC_{50} ~11 became ~2.1 in breast cancer cell line MCF7 after increasing lipophilicity).² The enantiopurity of this RPC also has been found to influence the cytotoxicity potential (IC_{50} ~9.5 μM for $\Delta\Delta\text{-}4^{4+}$, ~16.7 μM for $\Lambda\Lambda\text{-}4^{4+}$ in non-small cell lung carcinoma cell lines, H358 and H226) and maximum tolerable dose in mice (100 mg/kg mouse for $\Delta\Delta\text{-}4^{4+}$, 66 mg/kg

mouse for $\Lambda\Lambda\text{-4}^{4+}$).³ However, synthesis of enantiopure 4^{4+} has been very challenging because of the multiple intermediate steps and over-all low yield.

This thesis represents a simplified synthetic approach for enantioselective 4^{4+} with greater yield. RPCs have shown promise as photosensitizer in anticancer photodynamic therapy (PDT).²⁶ This thesis also shows that 4^{4+} is capable of inducing photocleavage when irradiated with blue light (470 nm) without the presence of reducing agent GSH. The stereo-selectivity also influences the rate of photocleavage reaction by inducing ~64%, ~57% and ~33% cleavage for supercoiled plasmid pUC18 DNA to produce circular plasmid DNA. Three types of radical ion scavengers including hydroxyl radical scavenger (mannitol, ethanol, sodium pyruvate), singlet oxygen scavenger (sodium azide) and metal or carbon-based radical scavenger (TEMPO) were used to indicate the radical species for photocleavage. Only TEMPO caused significant quenching in plasmid cleavage reaction which indicates that the responsible radical species is a metal or carbon-based radical. Based on the results a mechanism was proposed which says a metal based radical with highly oxidizing triplet excited state might be the cause of DNA strand secession by 4^{4+} .

Table of contents

Acknowledgement.....	iii
Abstract	iii
List of Illustrations.....	x
List of Tables.....	xii
List of Abbreviations.....	xiii
Chapter 1 Introduction.....	1
1.1 Challenges to develop successful chemotherapeutic agents.....	1
1.2 The role of metal based chemotherapeutic agents in treating cancer.....	1
1.3 Limitations of platinum based therapy.....	2
1.4 Ruthenium-based anticancer drugs.....	3
1.4.1 Ruthenium based anticancer drugs with labile ligands.....	3
1.4.2 Ruthenium polypyridyl complexes (RPCs).....	5
1.4.3 Selective cytotoxicity of RPCs.....	6
1.4.4 Influence of lipophilicity on RPCs.....	8
1.4.5 Influence of stereochemistry.....	9
1.4.6 Influence of redox chemistry.....	10
1.4.7 Use of RPCs in photodynamic therapy (PDT).....	10
1.4.8 Cellular compartment localization of RPCs.....	11
Scope of this dissertation.....	12
Chapter 2 A simplified synthetic approach to the enantiopure dimer $\Delta\Delta$ - and $\Lambda\Lambda$ - $[(\text{phen})_2\text{Ru}(\text{tatpp})\text{Ru}(\text{phen})_2]^{4+}$	13
2.1 Introduction.....	13
2.1.1. Established synthesis approach.....	15
2.1.2. Simplified synthetic approach.....	17

2.2 Experimental.....	17
2.2.1 Chemicals.....	17
2.2.2 Instrumentation.....	18
2.3 Synthesis of Enantiopure $[(\text{phen})_2\text{Ru}(\text{tatpp})\text{Ru}(\text{phen})_2]^{4+}$ ($\Delta\Delta\text{-4}^{4+}$).....	18
2.3.1 Resolution of $\Delta\text{-}[(\text{phen})_2\text{Ru}(\text{phendione})][\text{PF}_6]_2$ and $\Lambda\text{-}[(\text{phen})_2\text{Ru}(\text{phendione})][\text{PF}_6]_2$	18
2.3.2 Batch 1 : NMR scale synthesis of $\Delta\Delta\text{-}[(\text{phen})_2\text{Ru}(\text{tatpp})\text{Ru}(\text{phen})_2][\text{PF}_6]_4$	20
2.3.3 Batch 2: NMR scale synthesis of $\Delta\Delta\text{-}[(\text{phen})_2\text{Ru}(\text{tatpp})\text{Ru}(\text{phen})_2][\text{PF}_6]_4$	21
2.3.4 Synthesis of $\Delta\Delta\text{-}[(\text{phen})_2\text{Ru}(\text{tatpp})\text{Ru}(\text{phen})_2][\text{PF}_6]_4$	22
2.3.5 Metathesis reaction.....	23
2.3.6 Synthesis of $\Lambda\Lambda\text{-}[(\text{phen})_2\text{Ru}(\text{tatpp})\text{Ru}(\text{phen})_2][\text{PF}_6]_4$ and mix-- $[(\text{phen})_2\text{Ru}(\text{tatpp})\text{Ru}(\text{phen})_2][\text{PF}_6]_4$	23
2.4 Results and discussion.....	23
Chapter 3 Effect of stereochemistry on photocleavage.....	31
3.1 Photodynamic Therapy (PDT) and Photochemotherapeutics (PCT).....	31
3.2 Photo-activation of RPCs Influencing Biological Activity.....	31
3.3 Previous works regarding DNA photocleavage activity of $[(\text{phen})_2\text{Ru}(\text{tatpp})\text{Ru}(\text{phen})_2]^{4+}$ (4^{4+}).....	34
3.4 Experimental.....	34
3.4.1 Chemicals.....	34
3.4.2 Buffer preparation.....	35
3.4.3 DNA cleavage assay.....	36
3.4.4 Instrumentation for analyzing DNA cleavage %.....	37

3.5 Results and discussion.....	37
3.5.1 Photocleavage of 4 ⁴⁺ and effects of and stereochemistry.....	38
3.5.2 Active radical species responsible for photocleavage.....	43
3.6 Conclusion.....	47
References.....	49

List of Illustrations

Figure 1-1 Platinum based anticancer drugs.....	2
Figure 1-2 Ruthenium based anticancer drugs with labile ligands.....	4
Figure 1-3 [Ru(phen) ₃] ²⁺ (one of the parent RPCs).....	5
Figure 1-3 Selective cytotoxicity of RPCs.....	6
Figure 1-4 Ligand tatpp and some redox active RPCs (Ru-tatpp complexes).....	7
Figure 1-5 Two non-redox active RPCs.....	8
Figure 1-6 Influence of stereochemistry on IC ₅₀ values of RPCs in Non-small cell lung carcinoma cell line.....	9
Figure 1-7 Cellular compartment localization of RPCs detected by ICP-MS.....	11
Figure 2-1 Enantiomers of mononuclear RPCs.....	13
Figure 2-2 stereoisomers of dinuclear RPCs. (a) diastereomeric (meso) (b) enantiomeric.....	14
Figure 2-3 established synthetic route for ΔΔ-4 ⁴⁺	16
Figure 2-4 Sodium arsenyl tartrate.....	19
Figure 2-5 New simplified one-step synthesis scheme for enantiopure 4 ⁴⁺	25
Figure 2-6 ¹ H spectra of [(phen) ₂ Ru(tatpp)Ru(phen) ₂][PF ₆] ₄ in CD ₃ CN.....	27
Figure 2-7 ¹ H NMR spectra in DMSO-d ₆ for NMR scale reactions of batch 1.....	28
Figure 2-8 ¹ H NMR spectra in CD ₃ CN (tube F, J, K) and DMSO-d ₆ (tube L) of NMR scale reactions of batch 2.....	29
Figure 2-9 ¹ H NMR spectra in CD ₃ CN for the products obtained after overnight reflux and heating via new synthesis approach of ΔΔ-[(phen) ₂ Ru(tatpp)Ru(phen) ₂][PF ₆] ₄	30
Figure 3-1 (a) Two RPCs tested by Turro group (b) Ethidium bromide stained with agarose gels of the photocleavage of 100 μM pUC18 and 20 μM of the chloride salt of complex [Ru(bpy) ₂ (dppn)] ²⁺ in air.....	32

Figure 3-2(a) Photocleavage mechanism of $[(\text{phen})_2\text{Ru}(\text{phendione})]^{2+}$ at physiological pH (b) Ethidium bromide stained agarose gels showing photocleavage reactions of 0.154 nM pUC18 DNA bp and 27 μM of the hydrated $[(\text{phen})_2\text{Ru}(\text{phendione})]\text{Cl}_2$, irradiated at 470 nm for 2 h.....	33
Figure 3-3 <i>In vitro</i> DNA plasmid cleavage assay in which pUC19 DNA (154 μM DNA-bp) was incubated with 4^{4+} (31 μM) in PBS buffer (pH 7.2) and 1.0 mM GSH at varying $[\text{O}_2]$	38
Figure 3-4 Agarose gel (1.2%) stained with ethidium bromide showing DNA cleavage product of plasmid pUC18 DNA (0.154 mM DNA-bp) after treatment with 0.0128 mM RPC (mix- 4^{4+} , $\Delta\Delta$ - 4^{4+} and $\Lambda\Lambda$ - 4^{4+}) for 4 h incubation. All the lanes having “-” annotation were incubated in dark for 4 h and all the lanes with “+” annotation were incubated in 470 nm blue light for 4 h.....	39
Figure 3-5 Agarose gel (1.2%) stained with ethidium bromide showing DNA cleavage product of plasmid pUC18 DNA (0.154 mM DNA-bp) after treatment with 0.0128 mM RPC (mix- 4^{4+} , $\Delta\Delta$ - 4^{4+} and $\Lambda\Lambda$ - 4^{4+}). All the lanes having “-” annotation were incubated in dark for 1 h and all the lanes with “+” annotation were incubated in 470 nm blue light for 1h.....	40
Figure 3-6 Agarose gel (1.2%) stained with ethidium bromide showing DNA cleavage product of plasmid pUC18 DNA (0.154 mM DNA-bp) after treatment with 0.0128 mM RPC (mix- 4^{4+} , $\Delta\Delta$ - 4^{4+} and $\Lambda\Lambda$ - 4^{4+}). All the lanes having “-” annotation was incubated in dark for 30 min and all the lanes with “+” annotation was incubated in 470 nm blue light for 30 min.....	41
Figure 3-7 Average cleavage % (after applying correction factor 1.4 for circular pUC18 DNA/supercoiled pUC18 DNA) and standard deviation for mix- 4^{4+} , $\Delta\Delta$ - 4^{4+} and $\Lambda\Lambda$ - 4^{4+} after 30 min irradiation in 470 nm blue light and in dark	42
Figure 3-8 Agarose gel (1.2%) stained with ethidium bromide showing DNA cleavage product of plasmid pUC18 DNA (0.154 mM DNA-bp) after adding scavengers, after treatment with 0.0128 mM mix- 4^{4+} and irradiating in 470 nm blue light for 30 min.....	44
Figure 3-9 Electron transfer between 4^{4+} and DNA leading to DNA-base oxidation and photocleavage.....	45
Figure 3-10 Decrease in DNA photocleavage activity after addition of scavengers.....	46
Figure 3-11 Agarose gel (1.2%) stained with ethidium bromide showing DNA cleavage product of plasmid pUC18 DNA (0.154 mM DNA-bp) after treatment with 0.0128 mM $\Delta\Delta$ - 4^{4+} and $\Lambda\Lambda$ - 4^{4+} and irradiating in 470 nm blue light for 30 min.....	47

List of Tables

Table 2-1 Batch 1: NMR scale synthesis set up for $\Delta\Delta$ -[(phen) ₂ Ru(tatpp)Ru(phen) ₂][PF ₆] ₄	20
Table 2-2 Batch 2: NMR scale synthesis set up for $\Delta\Delta$ -[(phen) ₂ Ru(tatpp)Ru(phen) ₂][PF ₆] ₄	21
Table 3-1 Cleavage % for mix- 4 ⁴⁺ , $\Delta\Delta$ - 4 ⁴⁺ and $\Lambda\Lambda$ - 4 ⁴⁺ after 30 min (without correction factor)	42
Table 3-2 DNA cleavage reaction results of mix- 4 ⁴⁺ with various radical scavengers detected by densitometry	46

List of Abbreviations

AcOH	Acetic acid
ATM pathway	Ataxia telangiectasia mutated pathway
bp	Base-pair
bpy	2,2'-Bipyridine
BTAC	Benzene tetramine tetrahydrochloride
CD3CN	Deuterated acetonitrile
Cisplatin	cis-Diamminedichloroplatinum(II)
Dip	4,7-Diphenyl-1,10-phenanthroline
DMF	Dimethylformamide
DMSO	Dimethylsulfoxide
DNA	Deoxyribonucleic Acid
dppn	Benzo[i]dipyrido [3,2-a:2',3'-c]phenazine
dppz	Dipyrido[3,2-a: 2',3'-c]phenazine
ee%	Enantiomeric Excess
EI-MS	Electron Impact Ionization Mass Spectrometry
eq	Equivalent
EtOH	Ethanol
EDTA	Ethylenediaminetetraacetic Acid
GSH	Glutathione
γ H2AX	H2A histone family, member X
H-358	Human non-small cell lung cancer cells
HCC-2998	Human colon carcinoma cells
HPLC	High-performance liquid chromatograph
IC50	Half maximal inhibitory concentration
Im	Imidazole
In	Indazole

MeCN	Acetonitrile
MeOH	Methanol
MTD	Maximum tolerated dose
MTT	3-(4,5-Dimethylthiazol-2-yl)-2,5-diphenyltetrazolium bromide
NAMI-A	[ImH][trans-RuCl ₄ (DMSO)(Im)]
NHE	Normal hydrogen electrode
NMR	Nuclear Magnetic Resonance
phen	1,10-Phenanthroline
rac	Racemic
RPCs	Ruthenium Polypyridyl complexes
RT	Room temperature
tatpp	9,11,20,22-Tetraaza tetrapyrrodo[3,2-a:2'3'-c:3'',2''-1:2''',3''']-pentacene
TEMPO	(2,2,6,6-Tetramethylpiperidin-1-yl)oxyl
TMS	Tetramethylsilane
UV	Ultraviolet
32+	[(phen) ₂ Ru(tatpp)] ²⁺
44+	[(phen) ₂ Ru(tatpp)Ru(phen) ₂] ⁴⁺
4ph4+	[(ph ₂ phen) ₂ Ru(tatpp)Ru(ph ₂ phen) ₂] ⁴⁺

Chapter 1

INTRODUCTION

1.1 Challenges to develop successful chemotherapeutic agents

Cancer has become one of the leading lethal diseases globally, making the development of successful treatment options more and more necessary.⁴ Anti-cancer drug development has been one of the most expensive and time consuming process in the field of drug development. Anticancer chemotherapeutics has to qualify in some additional critical parameters besides going through all the conventional stages designed for drug development including preclinical and clinical trials. The establishment of a suitable therapeutic index (ratio of effective dose to toxic dose), selectivity for malignant cells, sensitivity towards different types of cancer and overcoming drug resistance are those additional challenges in the path of developing new anticancer agents and optimizing the existing treatment approaches.⁵

1.2 The role of metal based chemotherapeutic agents in treating cancer

Most of the chemotherapeutic agents that are approved by Food and Drug Administration (FDA) and currently in clinical use are organic in nature.⁴ However, metal-based anticancer medicines are also very potential candidates to treat a wide variety of malignancies.⁴ This class of drugs first took attention when “cisplatin” was found to be effective in treating testicular, ovarian, bladder, cervical, head and neck and small cell lung cancer.⁶ Cisplatin is a dichloro-diamino complex of platinum having square planar geometry. Due to the presence of labile ligands, it undergoes hydrolysis inside the body. The mono-aquated platinum product causes platinum binding to DNA, forming guanine-platinum adducts which can block replication or transcription leading to cancer cell death.^{6,7} Metallo-pharmaceuticals also offer some advantages over conventional organic

anticancer drugs which include wide range of coordination number, various geometries, suitable redox chemistry, various ligand substitution kinetics, 'tune-ability' of thermodynamics and various interaction modes with biological targets.⁴ Metal-based drugs can also be made more targeted towards cancer cells by incorporating photodynamic therapy (PDT) and by using suitable nanoparticle formulation as the drug delivery method.^{4,9} Besides platinum the other transition metals that have been tested for metal based chemotherapeutics include iron, ruthenium, rhodium, osmium, cobalt, gold and gallium.⁸

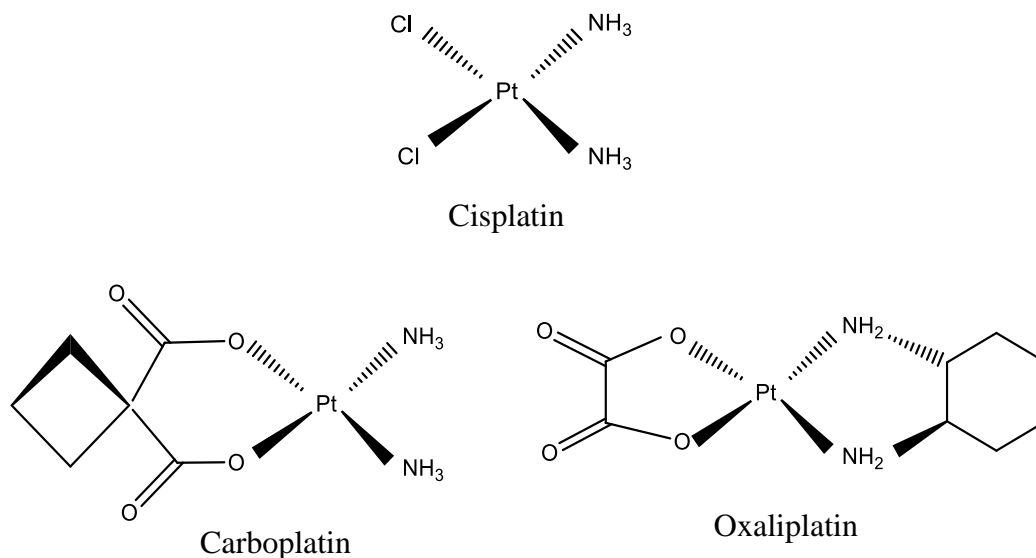


Figure 1-1 Platinum based anticancer drugs

1.3 Limitations of platinum based therapy

Regardless of the success of cisplatin, it comes with some severe drawbacks like nephrotoxicity, neurotoxicity, nausea, vomiting and hearing difficulties. It has also shown both intrinsic and acquired resistance towards many cancer types which made it effective

against only a narrow range of cancer types.⁷ Moreover, Cisplatin-therapy often fails to selectively target cancer cells and damage both the healthy and malignant cells.⁹ Two other platinum-based drugs in clinical use are oxaliplatin and carboplatin. Oxaliplatin has shown efficacy against many cisplatin resistant cancers¹⁰ and carboplatin has shown better patient tolerability.¹¹ Unfortunately, all three clinically approved platinum based drugs have been found to harm the healthy cells leading to severe side effects.⁹

1.4 Ruthenium-based anticancer drugs

Ruthenium (Ru) is the next most widely studied transition metal after platinum. It comes in the group 8 of the periodic table. The most common oxidation states for ruthenium based drugs are Ru (II), diamagnetic, d⁶ and Ru (III), paramagnetic, d⁵. A Ru (IV) is also possible but very rare due to the instability of such high oxidation state.⁴

1.4.1 Ruthenium based anticancer drugs with labile ligands

Drugs from this class having labile ligands, might contain a Ru (III) metal center.^{6,15} However, this Ru (III) needs to be reduced to Ru (II) oxidation state *in vivo* to exhibit anti-tumor activity. Triggering factors including low oxygen concentrations and high availability of cellular reducing agent glutathione (GSH) are regarded responsible to cause the Ru (III) to Ru (II) conversion *in vivo*.^{12, 13, 14}

The journey of ruthenium based metallo-pharmaceuticals having labile ligands like cisplatin, started in 1980s when Clarke and coworkers reported the anticancer activity of *fac*-[RuCl₃(NH₃)₃] in mice. The real breakthrough in this field was the discovery of the complex imidazolium *trans*-[tetrachloridobis(1H-imidazole)ruthenate (III)] (KP418) by Keppler and coworkers in 1986. This molecule showed therapeutic activity against murine p388 and B16 melanoma.¹⁵ The further development of this was indazolium *trans*-

[tetrachloridobis(1H-imidazole)ruthenate (III)] (KP1019) and imidazolium *trans*-[tetrachlorido(1H-imidazole)(S-dimethyl sulfoxide) ruthenate (III)] (NAMI-A) which entered clinical trial in 2003 and 1999, respectively.⁶ However, NAMI-A was discarded from being

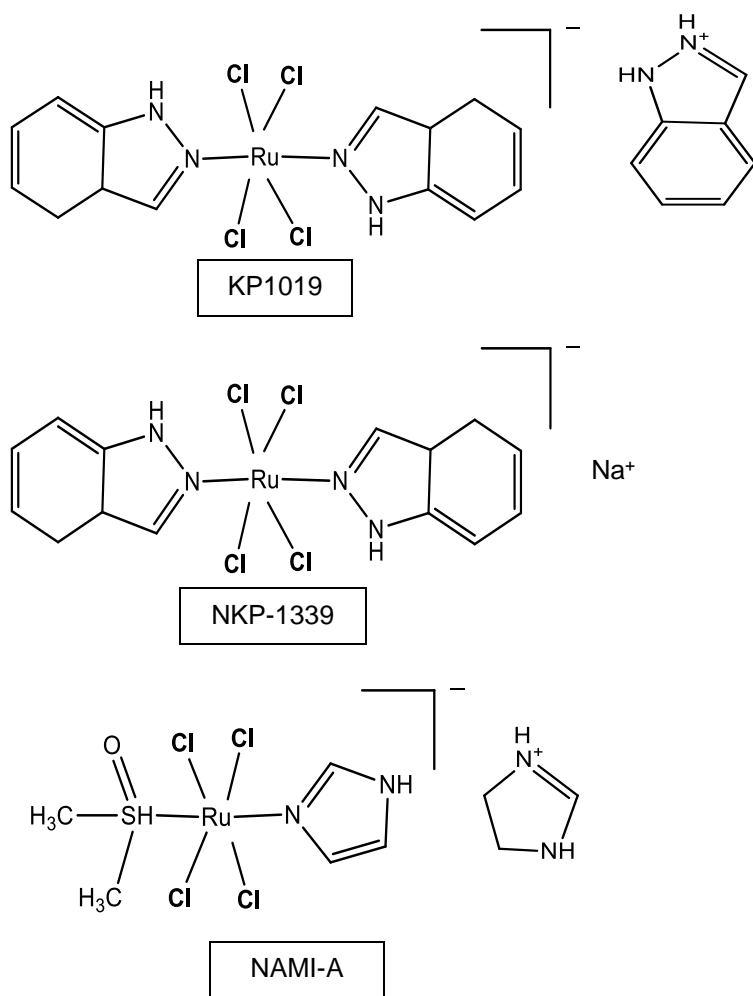


Figure 1-2 Ruthenium based anticancer drugs with labile ligands

developed as an anticancer therapeutic because of phase I and phase II clinical trial results which indicated this to be less effective in stopping disease progression and to cause partial response.⁴ Most recently, NKP-1339 (a sodium salt analogue of KP1019)

has proceeded to phase I trials. All of these compounds have labile ligands and become subjected to hydrolysis inside the body.¹⁵

1.4.2 Ruthenium polypyridyl complexes (RPCs)

Another class of ruthenium-based metal complexes showing promise are ruthenium polypyridyl complexes (RPCs), such as $[\text{Ru}(1,10\text{-phenanthroline})_3]^{2+}$ and related analogues. The biological activity of these RPCs was first studied by Dwyer and coworkers in the late 1950's and early 60's.^{16,17} Unlike cisplatin, NKP-1339, and NAMI-A, RPCs lack labile ligands and the entire complex is the bioactive unit.¹⁶ $[\text{Ru}(3,4,7,8\text{-tetramethyl-1,10-phenanthroline})_3]^{2+}$ from this class was shown to inhibit dispersed tumor cell growth in mice.¹⁷ Also, 99% of the radio-labeled $[\text{Ru}(1,10\text{-phenanthroline})_3]^{2+}$ was found in the urine of subjected mice showing the complex is ultimately excreted in urine intact.¹⁸ While a start, the limited anti-cancer activity and potent inhibition of acetylcholine esterase (AChE)¹⁶ leading to neurotoxicity limited the utility of $[\text{Ru}(1,10\text{-phenanthroline})_3]^{2+}$.

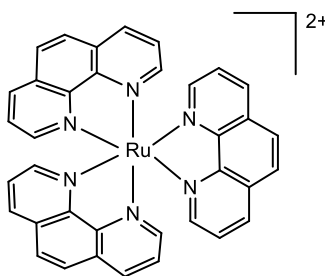


Figure 1-3 $[\text{Ru}(\text{phen})_3]^{2+}$ (one of the parent RPCs)

Phen = 1, 10-Phenanthroline

However, new but related RPCs have shown tremendous potential as anti-cancer drugs with greater and more selective cytotoxicity towards malignant cell lines,

low neurotoxicity in mice, and demonstrable anti-tumor activity in vivo. RPCs possess some of the attractive characteristics for which they are considered promising anti-cancer leads.⁴ These characteristics include lipophilicity and cellular uptake of the molecule, ability to enter different cell compartments, selective toxicity towards malignant cells, stereochemistry and redox chemistry.^{1,2,3,4} They are capable of binding biological targets electrostatically and also by intercalating with DNA.¹⁹

1.4.3 Selective cytotoxicity of RPCs

RPCs can be more selective to kill malignant cells than healthy cells. A recent report published from the MacDonnell's group is a good example of this particular case. Two RPCs **4⁴⁺** and **3²⁺** (figure 1-4) were tested on a number of malignant cell lines including MCF7 (breast cancer cell line), H358 (non-small cell lung carcinoma cell line), CCL228 (colon cancer cell line) and a healthy cell line MCF10 (breast epithelial tissue). The RPCs **4⁴⁺** and **3²⁺** were selectively cytotoxic to malignant cell lines compared to a standard drug cisplatin² (figure 1-40).

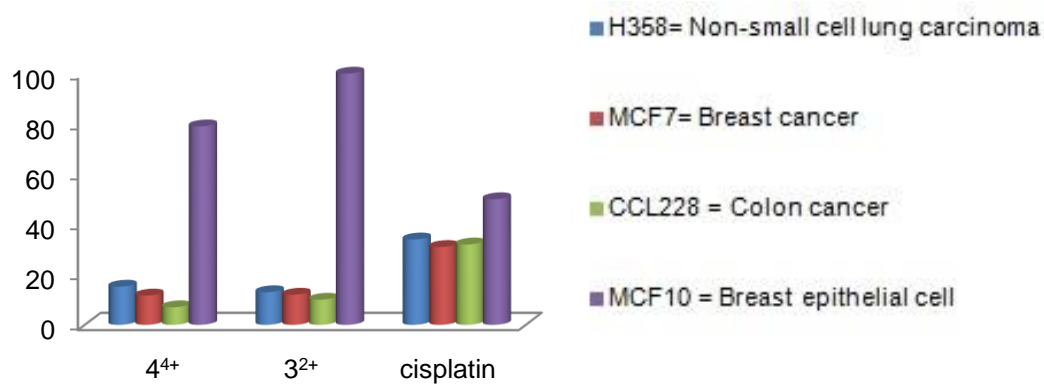


Figure 1-3 Selective cytotoxicity of RPCs

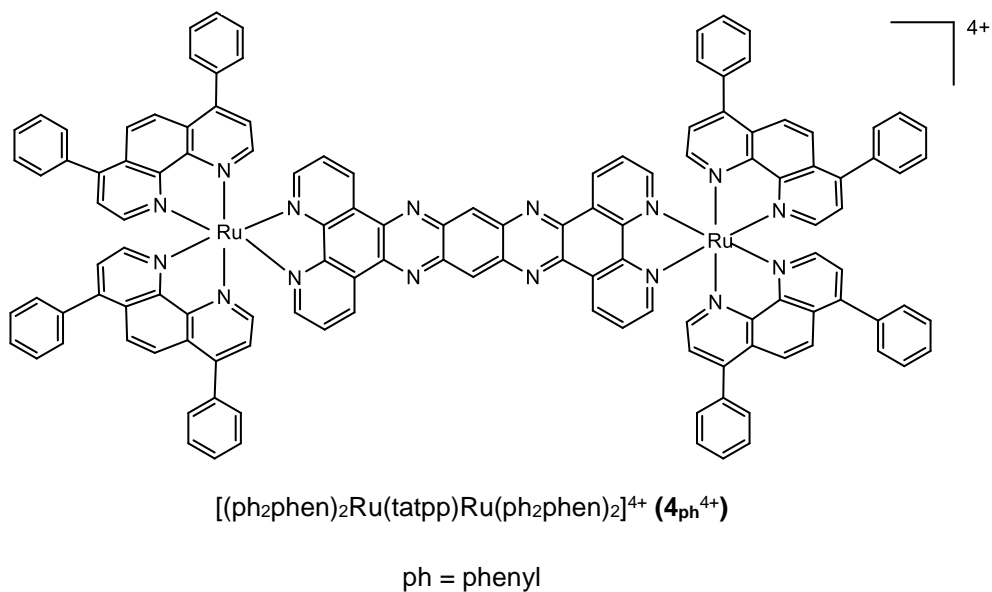
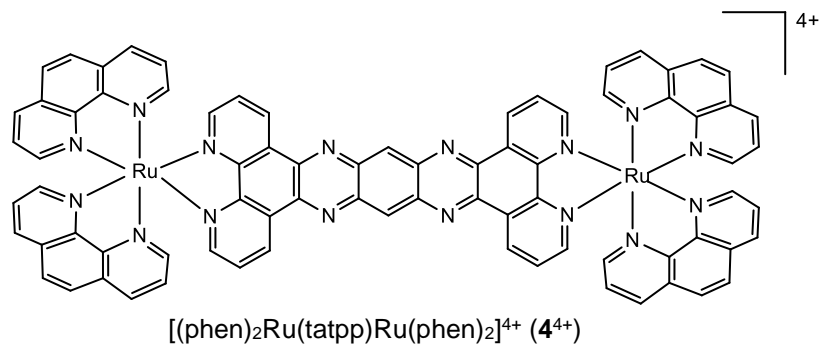
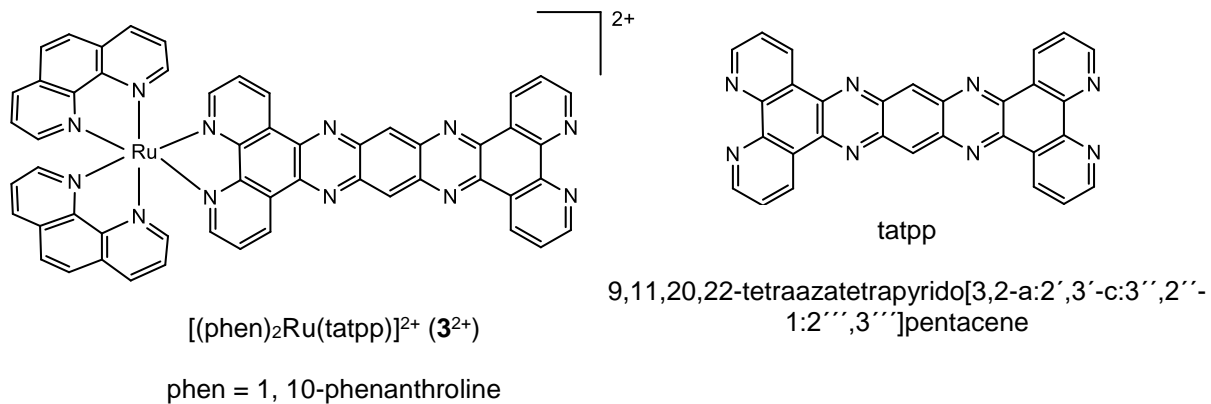


Figure 1-4 Ligand tatpp and some redox active RPCs (Ru-tatpp complexes)

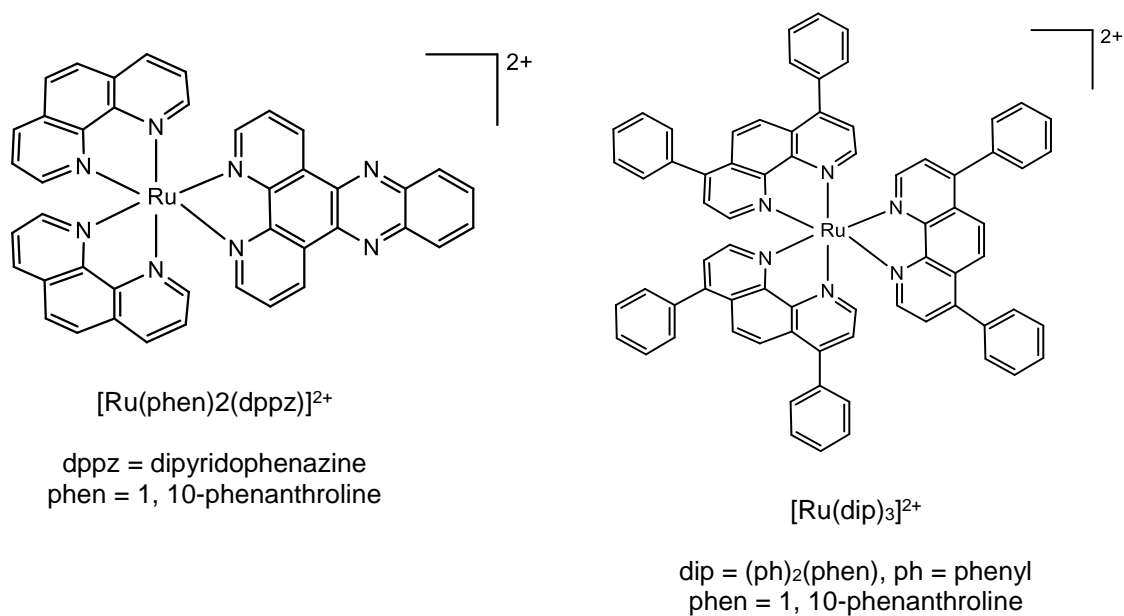


Figure 1-5 Two non-redox active RPCs

1.4.4 Influence of lipophilicity on RPCs

Lipophilicity is an important attribute for drugs for successful cellular uptake. Barton and his group investigated the relationship between lipophilicity and cellular uptake with RPCs containing dppz ligands.⁴ They reported a compound called Δ -[Ru(bpy)₂(dppz)]²⁺ capable of binding oligonucleotides but incapable of permeating cell membranes due to poor lipophilicity. Later they observed cellular uptake for the complex when the bpy ligands were replaced with more lipophilic dip ligands. From the complexes studied by Barton and his group, the highest cellular uptake was seen for the most lipophilic ligand containing RPC.⁴ Gill *et al*, also showed that modifying the lipophilicity of polypyridyl ligands can greatly influence the cytotoxicity and intercellular targets for Ru (II) complexes.²⁰ Currently, the MacDonnell's group has reported two redox active RPCs which show remarkable increase in cytotoxicity potentials and tolerable dose (in mice)

after increasing lipophilicity of the terminal polypyridyl ligands. One of those RPCs is the complex 4^{4+} with a selectivity index of 7. The selectivity index was determined by the ratio of IC_{50} of healthy cells (MCF10) to IC_{50} of malignant cells (MCF7). The selectivity index became 11 when the 1, 10 phenanthroline ligands were replaced with diphenylphenanthroline ligands (figure 1-4).²

1.4.5 Influence of stereochemistry on RPCs

Stereochemistry is also very closely related to the biological impacts of RPCs. From the parent RPCs studied by Dwyer and his team, stereo-selectivity has been found to play crucial role in determining tolerable dose, cytotoxicity profile and enzyme inhibition activity.¹⁶ The study regarding the binding affinities of $[Ru(phen)_3]^{2+}$ revealed that the Δ -isomer tends to preferentially bind GC base pair and the Λ -isomer tends to preferentially bind the AT base pairs of DNA.²¹ According to the report of Zeng *et al*, chiral selectivity can significantly influence the inter-cellular localization of RPCs.²² The MacDonnell's lab showed that the maximum tolerable dose in mice and cytotoxicity in malignant cell lines can also be very different for the complex 4^{4+} and 3^{2+} from figure 1-6 is representing this results.³

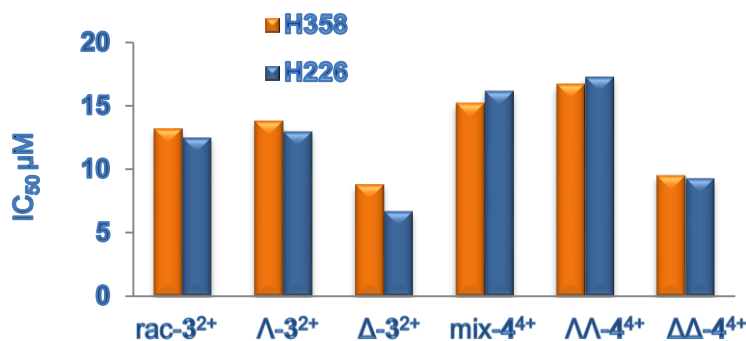


Figure 1-6 Influence of stereochemistry on IC_{50} values of RPCs in Non-small cell lung carcinoma cell line

1.4.6 Influence of redox chemistry on RPCs

Some RPCs are capable of undergoing redox cycling *in vivo* and producing reactive oxygen species (ROS) to cause cell death. For undergoing this kind of redox cycling the first reduction potential should be accessible by common cellular reducing agents like glutathione. The complex $[(\text{phen})_2\text{Ru}(\text{tatpp})\text{Ru}(\text{phen})_2]^{4+}$ (4^{4+}) is an example of such redox active RPCs with a first reduction potential (-0.02 V vs NHE) accessible to be reduced by the GSH (reduction potential -0.24 V vs NHE, pH 7).^{1,2} This complex has been established to cause DNA cleavage by producing hydroxyl radicals (OH^\cdot). The redox cycling is located on the ligand tatpp and mediated by the $[\text{GSH}] / [\text{O}_2]$ in a low oxygen environment.¹ This particular mode of action gives this molecule an added advantage to be effective in hypoxic tissue environment (tumor cells) without any photoexcitation from external source.^{1,3}

1.4.7 Use of RPCs in photodynamic therapy (PDT)

PDT is a powerful tool for targeted cytotoxicity to cancer cells.⁹ PDT works primarily by producing ROS, especially OH^\cdot (hydroxyl radicals) $^1\text{O}_2$ (singlet oxygen) and both OH^\cdot and $^1\text{O}_2$ can directly damage cancer cells.²³ RPCs can be successfully used as photosensitizers in PDT. Turro and Sadler's pioneering works have shown light irradiation of some RPCs can lead to RPC-DNA adduct formation. In such cases, the RPC undergoes ligand dissociation due to photoexcitation and form covalent bonds with DNA.^{24,25} Later on, Turro and his group have reported RPCs causing both ligand dissociation and $^1\text{O}_2$ production.²⁶ Some promising RPCs from the Turro's group have also been discussed in chapter 3. The Glazer group has developed sterically clashing ligands containing RPCs which undergo specific ligand ejection upon irradiation with visible light >400 nm and cause covalent modification of DNA. This approach was

hypothesized to be effective in oxygen deficient cancer cells the Glazer group.²⁷⁻²⁹ The McFarland's group developed RPCs with the lowest lying ³IL triplet excited states and remarkably longer excited state life times (22 – 270 μs) by modifying the polypyridyl ligands.³⁰⁻³³ The RPCs from the McFarland's group were designed to have a low lying ³IL excited state and high ¹O₂ quantum yield after interaction with biological target. These complexes interacted with DNA leading to DNA photocleavage and highly potent photocytotoxicity in two cultured malignant cell lines (HL60 and melanoma cell lines).³²

1.4.8 Cellular compartment localization of RPCs

RPCs can be accumulated in different cellular cell components including nucleus, mitochondria or lysosomes.⁴ In spite of the fact that a number of RPCs can bind DNA by intercalation¹⁹ some ruthenium polypyridyl complexes can be accumulated preferentially in other subcellular organelles rather than accumulating in nucleus.⁴ The MacDonnell's group conducted an experiment with both redox active and non-redox active RPCs and found completely different cellular localization pattern for each of them (figure 1-7).³⁴

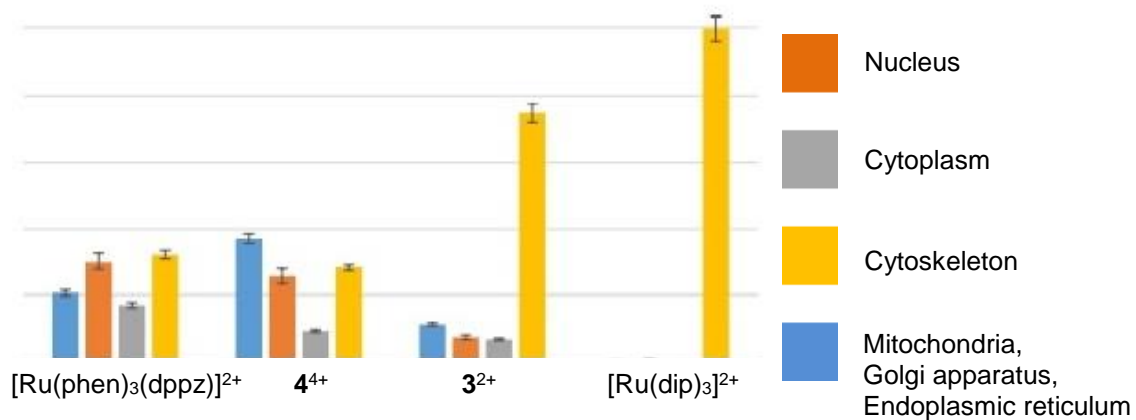


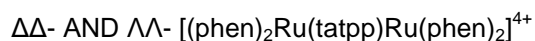
Figure 1-7 Cellular compartment localization of RPCs detected by ICP-MS

Scope of this dissertation

The RPCs, **4⁴⁺** and **3²⁺** have shown promise as potential anticancer chemotherapeutic leads. They have been reported to cleave DNA (cell free plasmid cleavage assay), selectively cytotoxic in malignant cell lines (cellular MTT assay) and well tolerated in mice (67 mg/kg mouse in animal toxicity study). Also, the $\Delta\Delta$ -**4⁴⁺** and Δ -**3²⁺** has been found to cause 83% growth regression of non-small cell lung carcinoma xenografts in nude mice. Considering the valuable *in vivo* anticancer activity results, a new and more efficient synthesis route was necessary to synthesize enantiopure **4⁴⁺** as the established route is time consuming and gives low yield. This thesis represents a simplified synthetic approach for the enantiopure **4⁴⁺** with greater yield in chapter 2. Chapter 3 represents the experiments designed to reveal the photocleavage potentials of **4⁴⁺**. Chapter 3 also shows the experiments focused to determine the effects of stereochemistry on the rate of photocleavage and the radical species which cause the photocleavage reaction.

Chapter 2

A SIMPLIFIED SYNTHETIC APPROACH TO THE ENANTIOPURE DIMER



2.1 Introduction

RPCs are chemically stable and coordinatively saturated Ru(II) complexes with a low spin d^6 electronic configuration.¹ RPCs with three identical bidentate diimine ligands have a D_3 octahedral symmetry and exist as enantiomers. The three bidentate ligands spiral around the three-fold rotation axis giving a helical structure for this class of compounds. Conventionally, the Greek character “ Δ ” stands for “right handed helix” and “ Λ ” stands for “left handed helix” depicting how the three ligands cant along the screw axis. (Figure 2-1)

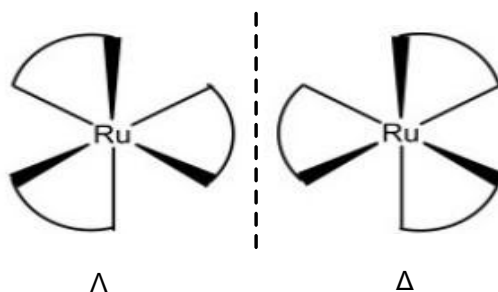


Figure 2-1 Enantiomers of mononuclear RPCs

These Δ and Λ enantiomers are non-superimposable mirror images of each other. If two such metal centers having three bidentate ligands can be joined together by a symmetric bridging ligand like tatpp, symmetric binuclear RPCs can be formed. These RPCs have three stereochemical configurations; a pair of enantiomers $\Delta\Delta$ and $\Lambda\Lambda$ and the meso compound $\Delta\Lambda$ which is identical to $\Lambda\Delta$ (Figure 2-2), contains an internal mirror plane and is achiral. When the syntheses of the dimer is done without controlling the

chirality at the metal centers, a statistical mixture of 25% $\Delta\Delta$, 25% $\Lambda\Lambda$, and 50% meso $[(\text{phen})_2\text{Ru}(\text{tatpp})\text{Ru}(\text{phen})_2]^{4+}$ is obtained.

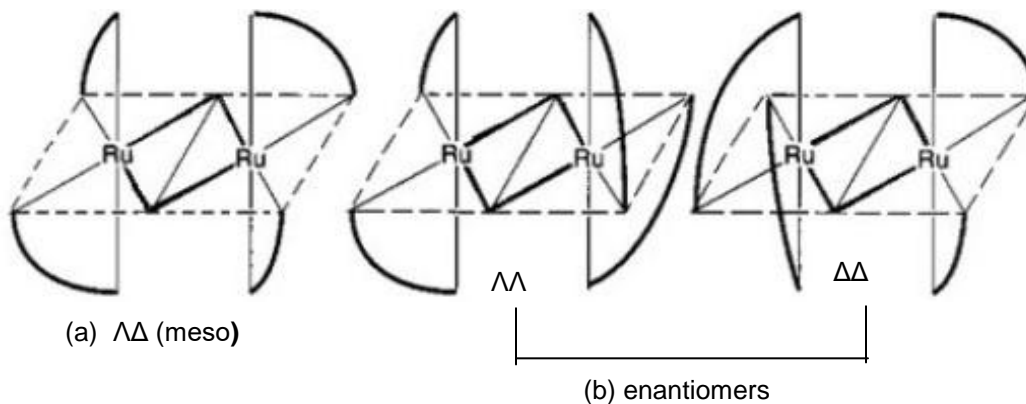


Figure 2-2 stereoisomers of dinuclear RPCs. (a) diastereomeric (meso)

(b) enantiomeric

The chemical nature and biological roles of RPCs, especially $[\text{Ru}(\text{phen})_3]^{2+}$ was studied extensively during 1960s by Dwyer and co-workers.^{16,17} They also investigated the relationship between chirality and biological activities of RPCs like maximum tolerable dose and enzyme inhibition potential. They found the complex $[\text{Ru}(\text{phen})_3]^{2+}$ as a potent neurotoxin as they inhibit an important enzyme called acetyl choline esterase (AChE).¹⁶ Interestingly, the binding propensity and enzyme inhibition % were significantly different for two enantiomers. The Δ -enantiomer inhibited 90% of the enzyme where the Λ -enantiomer only inhibited 20%.¹⁶ Later, the DNA binding affinities for this set of enantiomers were also observed to be remarkably different. RPCs with large planar ligand, such as dppz, are capable of binding DNA via intercalation.²⁶ The binding constants for the two enantiomeric forms of $[(\text{phen})_2\text{Ru}(\text{dppz})]^{2+}$ were found different, $3.2 \times 10^6 \text{ M}^{-1}$ for Δ -form and $1.7 \times 10^6 \text{ M}^{-1}$ for the Λ -form.^{35,36,37} Yadav *et al.* reported the

influence of stereoselectivity of RPCs by investigating the IC₅₀ values in non-small cell lung carcinoma cell lines.³

The MacDonnell group has established that the complex [(phen)₂Ru(tatpp)Ru(phen)₂]⁴⁺ (**4**⁴⁺) binds to duplex DNA via intercalation with a binding constant of ~ 3.8 X 10⁵ M⁻¹ at 298 K.³⁸ The stereochemistry of this compound also influences its ability to kill malignant cells. The ΔΔ-form was found to be more cytotoxic (IC₅₀ ~ 9.5 μM) towards non-small cell lung carcinoma cell line H358 compared to the ΛΛ-enantiomeric form (IC₅₀ ~ 16.7 μM).³ Also the ΔΔ-[(phen)₂Ru(tatpp)Ru(phen)₂]⁴⁺ was found to cause 83% growth suppression of human non-small cell lung carcinoma in nude mice xenograft models.³

2.1.1 Established synthesis approach

The three-step synthetic procedure for enantiopure [(phen)₂Ru(tatpp)Ru(phen)₂]⁴⁺ has already been established by the MacDonnell's lab.² Essentially, the starting complex [Ru(phen)₂(phendione)]²⁺ is resolved into the Δ and Λ enantiomers using diastereoselective precipitation upon treatment with sodium arsenyl-D(-)-tartrate or sodium arsenyl-L(+)-tartrate, the structure of which is shown in figure 2-4. This enantiopure starting material is then used to build a tatpp ligand between two such units. The overall synthetic procedure consists of three steps and is shown in Figure 2-3 and gives enantiopure ΔΔ- or ΛΛ- [(phen)₂Ru(tatpp)Ru(phen)₂]⁴⁺ in a 33% overall yield. In step 1, the desired enantiomer of [Ru(phen)₂(phendione)]²⁺ is reacted with 1,2-diamino-4,5-dinitrobenzene in ethanol to yield the dinitrodppz complex. In step 2, hydrogenation of the [Ru(phen)₂(dinitrodppz)]²⁺ yields [Ru(phen)₂(diaminodppz)]²⁺, and while this step appears straightforward, it is often difficult to drive the hydrogenation to completion. The final step involves the coupling of [Ru(phen)₂(phendione)]²⁺

with $[\text{Ru}(\text{phen})_2(\text{diaminodppz})]^{2+}$ which gives crude yields in the range of 50-60%. Further purification via silica column chromatography results in further losses, ultimately giving an isolated yield of 33%.^{2,39,40,41}

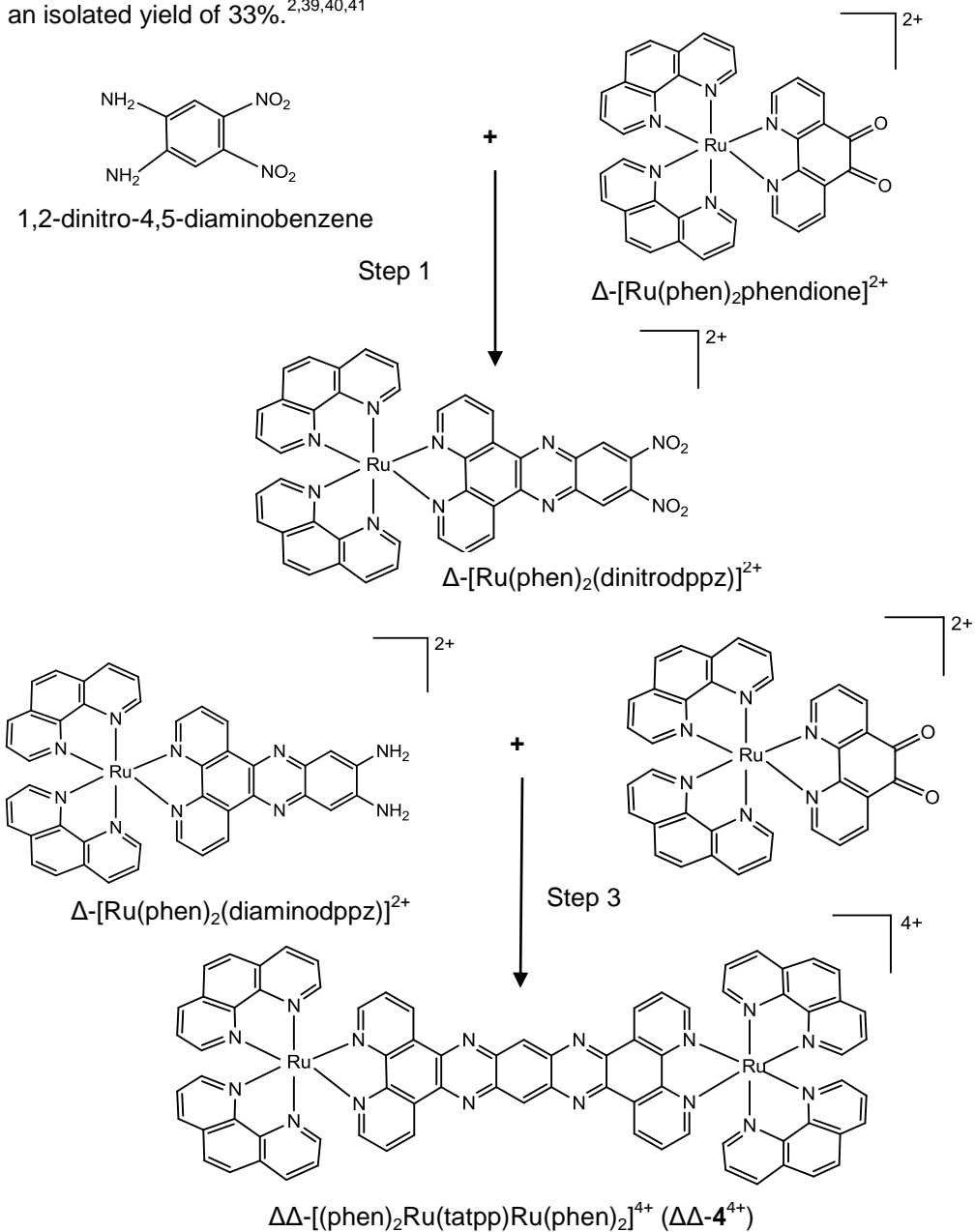


Figure 2-3 established synthetic route for $\Delta\Delta$ -4⁴⁺

2.1.2 Simplified synthetic approach

Early attempts to directly prepare $[(\text{phen})_2\text{Ru}(\text{tatpp})\text{Ru}(\text{phen})_2]^{4+}$ from the condensation reaction of two equivalents of $[\text{Ru}(\text{phen})_2(\text{phendione})]^{2+}$ and one equivalent of 1,2,4,5-tetraaminebenzene hydrochloride (BTAC) never gave any hint of the desired product in the crude reaction isolate. The reason for that might be due to the poor purity of the BTAC which is sold as a technical grade product (95% pure) from Sigma-Aldrich. Attempts to purify the BTAC by recrystallization resulted in huge losses.

Given the simplicity of this approach, we decided to re-examine this reaction with a systematic approach to optimizing reaction conditions and solvents. This chapter describes this study and our eventual success in developing this streamlined and very straightforward approach to the desired product. Moreover, when conducted with enantiopure $[\text{Ru}(\text{phen})_2\text{phendione}]^{2+}$, the enantiopure dimer was obtained.

We designed five NMR scale reactions in the batch 1 to examine the role of solvent type and base (K_2CO_3 or NaOAc). Solvents examined include ethanol, DMSO (dimethyl sulfoxide) and glacial acetic acid. All initial tests were done at room temperature and we wanted to see if refluxing conditions, which are typically used, were warranted. The batch 2 NMR experiments was designed considering the results from batch 1. Finally, large scale reaction conditions were examined to see how all the NMR scale reactions could be scaled up.

2.2 Experimental

2.2.1 Chemicals

Ruthenium (III) chloride was purchased from Pressure Chemical Co (Pittsburg, PA). Benzenetetramine tetrahydrochloride (BTAC), diethyl formamide, 1, 10-phenanthroline (phen), tetra-n-butyl ammonium chloride, , L-(+)-tartaric acid, D-(-)-tartaric

acid were purchased from Aldrich. Potassium carbonate anhydrous (K_2CO_3) and lithium chloride anhydrous (LiCl) and sodium acetate (NaOAc) were purchased from the Malinckrodt and Alfa Aesar and Fisher Scientific respectively. NH_4PF_6 (ammonium hexafluorophosphate) was bought from Oakwood Chemicals (Estill, SC). Acetic acid glacial from EMD Milipore Corporation, dimethyl sulfoxide (DMSO) from Macron and ethanol from Deconl were purchased and used as received. 1, 10-phenanthroline-5,6-dione (phendione),⁴² $Ru(phen)_2Cl_2$,⁴³ $[(phen)_2Ru(phendione)][PF_6]_2$ ref and $[(phen)_2Ru(phendione)](PF_6)_2$,⁶⁰ sodium arsenyl-D-(-)-tartrate⁴⁴ and sodium arsenyl-L-(+)-tartrate⁴⁴ were prepared according to the literature procedure. All deuterated solvents used for NMR analysis were purchased from Cambridge Isotope Laboratories Inc.

2.2.2 Instrumentation

1H spectra for all the synthesized compounds were taken in JOEL Eclipse Plus 500 MHz. The NMR solvents used were CD_3CN , D_2O , $DMSO-d_6$ or CD_3Cl . The spectrophotometer is referenced to $(Me)_4Si$ as the standard and all the chemical shifts are reported in ppm. The enantiomeric excess (ee%) was determined using a HPLC-LARIHC-CF -RN column with a mobile phase consisting of methanol and MeCN (methanol : MeCN = 95 : 5, 0.07 M ammonium nitrate, NH_4NO_3).

2.3 Synthesis of Enantiopure $[(phen)_2Ru(tatpp)Ru(phen)_2]^{4+}$ ($\Delta\Delta-4^{4+}$)

2.3.1 Resolution of $\Delta-[(phen)_2Ru(phendione)][PF_6]_2$ and $\Lambda-[(phen)_2Ru(phendione)][PF_6]_2$

The Δ and Λ isomers of $[(phen)_2Ru(phendione)][PF_6]_2$ were isolated with a slight modification from the literature procedure.⁴⁵ Racemic $[(phen)_2Ru(phendione)]Cl_2$ (1.0 g) and 2.25 g of sodium arsenyl-D-(-)-tartrate were dissolved separately in 25 and 30 mL of

hot water, respectively. The solution of sodium arsenyl-D-(-)-tartrate was added to the solution of $[(\text{phen})_2\text{Ru}(\text{phendione})]\text{Cl}_2$ stirred for 30 minutes and chilled overnight at 4°C . The precipitate obtained predominantly contained Δ -form of the complex and the filtrate was rich in Λ -form. The precipitate was then washed with water and treated with 2 M nitric acid to decompose arsenyl tartrate. Next, a saturated aqueous solution of NH_4PF_6 is added to obtain Δ - $[(\text{phen})_2\text{Ru}(\text{phendione})][\text{PF}_6]_2$. However, two such resolution cycles were required to get an enantiomeric excess (ee%) of $> 95\%$. The Λ -form rich filtrate was further treated with a solution of sodium arsenyl-L-(+)-tartrate, chilled overnight and converted to Λ - $[(\text{phen})_2\text{Ru}(\text{phendione})][\text{PF}_6]_2$ in the same fashion as Δ - $[(\text{phen})_2\text{Ru}(\text{phendione})][\text{PF}_6]_2$. Finally, Λ - $[(\text{phen})_2\text{Ru}(\text{phendione})][\text{PF}_6]_2$ was washed with water and dried in vacuum oven at 60°C for 30 minutes. We observed that, one resolution cycle was enough to obtain the Λ -form with an enantiomeric excess (ee%) of $> 95\%$.

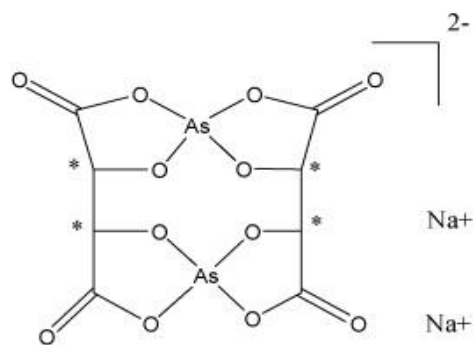


Figure 2-4 Sodium arsenyl tartrate

2.3.2 Batch 1: NMR scale synthesis of $\Delta\Delta$ -[(phen)₂Ru(tatpp)Ru(phen)₂][PF₆]₄

A 6.93 mM stock solution of Δ -[(phen)₂Ru(phendione)][PF₆]₂ was prepared by dissolving in MeCN. BTAC stock solution was prepared with a concentration of 26.1 mM by dissolving in DMSO-d₆. We designed 5 small scale reactions in five NMR tubes in such a way that provides the final molar ratio for Δ -[(phen)₂Ru(phendione)][PF₆]₂ and BTAC to be 2:1 in each tube designated as A – E in Table 2-1. The other chemicals and solvents used to optimize the reaction were added following the amounts stated in Table 2-1 and stirred overnight at room temperature.

Table 2-1 Batch 1: NMR scale synthesis set up for $\Delta\Delta$ -[(phen)₂Ru(tatpp)Ru(phen)₂][PF₆]₄

	A	B	C	D	E
Δ -[(phen) ₂ Ru(phendione)][PF ₆] ₂	750 μ L				
BTAC	100 μ L				
K ₂ CO ₃		~15 mg	~15 mg		~15 mg
NaOAc				~15 mg	
Ethanol	650 μ L	650 μ L		650 μ L	
DMSO-d ₆			650 μ L		
Acetic Acid					650 μ L

After overnight stirring, ¹H NMR spectroscopy was performed to characterize the product. The obtained ¹H NMR spectra were matched with a previously reported ¹H NMR spectra for $\Delta\Delta$ -[(phen)₂Ru(tatpp)Ru(phen)₂][PF₆]₄.

2.3.3 Batch 2: NMR scale synthesis of $\Delta\Delta$ -[(phen)₂Ru(tatpp)Ru(phen)₂][PF₆]₄:

The data obtained from Batch 1 suggested that tube E had the most optimum reaction conditions. So in the next batch, seven more tubes were prepared in a similar fashion of Batch 1, each having Δ -[(phen)₂Ru(phendione)][PF₆]₂ dissolved in MeCN (750 μ L), BTAC dissolved in DMSO-d₆ (750 μ L), ~15 mg of K₂CO₃ and 650 μ L of acetic acid glacial (designated F – J in Table 2-2). For tubes F – J, different BTAC stock solutions were prepared so that the final molar ratio of Δ -[(phen)₂Ru(phendione)][PF₆]₂ to BTAC decrease from 2:1 to 1.4:2. Tube K had (~30 mg K₂CO₃) and tube L had the [(phen)₂Ru(phendione)][PF₆]₂ dissolved in DMSO-d₆ instead of MeCN. For, tube J, the ¹H NMR spectra taken in CD₃CN was identical with the literature spectra (Figure 2-6)

Table2-2 Batch 2: NMR scale synthesis set up for $\Delta\Delta$ -[(phen)₂Ru(tatpp)Ru(phen)₂][PF₆]₄

	Molar ratio of Δ -[(phen) ₂ Ru(phendione)][PF ₆] ₂ : BTAC
F	2.2:1 (~ 15 mg K ₂ CO ₃)
G	2.0:1 (~ 15 mg K ₂ CO ₃)
H	1.8:1 (~ 15 mg K ₂ CO ₃)
I	1.6:1 (~ 15 mg K ₂ CO ₃)
J	1.4:1 (~ 15 mg K ₂ CO ₃)
K	2:1 (~ 30 mg K ₂ CO ₃)
L	2.1 (~ 15 mg K ₂ CO ₃) (Δ -[(phen) ₂ Ru(phendione)][PF ₆] ₂ dissolved in DMSO-d ₆)

2.3.4 Synthesis of $\Delta\Delta$ -[(phen)₂Ru(tatpp)Ru(phen)₂][PF₆]₄

100 mg of Δ -[(phen)₂Ru(phendione)][PF₆]₂ (104 μ mol) was dissolved in 15 mL of MeCN and 24.5 mg (87 μ mol) of BTAC was dissolved in 2 mL of DMSO. These two solutions were added to a 50 mL round bottom flask containing ~450 mg of K₂CO₃. Finally the volume was made 30 mL by adding 13 mL of acetic acid. The reaction mixture was left to stir overnight at room temperature. One small aliquot of ~1 mL was taken from the reaction mixture to characterize it by ¹H NMR spectroscopy. The NMR solvent used was CD₃CN and the obtained ¹H NMR spectra was identical to a previously published ¹H NMR spectra for $\Delta\Delta$ -[(phen)₂Ru(tatpp)Ru(phen)₂][PF₆]₄ in all aspects.³⁹

We repeated this procedure multiple times and in most cases the reaction was complete within 20 hours for $\Delta\Delta$ -[(phen)₂Ru(tatpp)Ru(phen)₂][PF₆]₄. However, in few cases, the ¹H NMR spectra showed presence of starting material or reaction intermediates. In those cases, around 6 mg of BTAC and 100 mg of K₂CO₃ were added to the reaction mixture and let it stir for some more time. In every 12 hours, a small aliquot of ~1 mL was taken from the reaction mixture and the ¹H NMR spectra was checked to confirm that the reaction was complete before doing the work up. During the work up, MeCN was removed from the reaction mixture by rotovap drying. The resulting concentrated solution was filtered with a frit filter having an additional layer of celite to minimize product loss. Celite captured the $\Delta\Delta$ -[(phen)₂Ru(tatpp)Ru(phen)₂][PF₆]₄. The product is gained from the celite layer by washing with small amount of MeCN. The resulting solution is concentrated enough by rotovapping. Finally the $\Delta\Delta$ -[(phen)₂Ru(tatpp)Ru(phen)₂][PF₆]₄ was precipitated from the concentrated solution by adding saturated aqueous NH₄PF₆ solution to it. The ¹H NMR spectra in CD₃CN was confirmed by matching with literature spectra. The average yield was 63%.

2.3.5 Metathesis reaction

The $\Delta\Delta$ -[(phen)₂Ru(tatpp)Ru(phen)₂(PF₆)₄] was dissolved in acetone and converted to $\Delta\Delta$ -[(phen)₂Ru(tatpp)Ru(phen)₂Cl₄] by dropwise addition of tetra butyl ammonium chloride dissolved in acetone. The ¹H NMR spectra in CD₃CN was confirmed by matching with literature spectra. The average yield was 59%.

2.3.6 Synthesis of $\Lambda\Lambda$ -[(phen)₂Ru(tatpp)Ru(phen)₂][PF₆]₄ and mix-(phen)₂Ru(tatpp)Ru(phen)₂][PF₆]₄

Both $\Lambda\Lambda$ and mix[-(phen)₂Ru(tatpp)Ru(phen)₂][PF₆]₄ can be synthesized following exactly the same procedure for the $\Delta\Delta$ -form, by taking Λ or racemic form of [(phen)₂Ru(phendione)][PF₆]₂ as the starting material. In most of the times, the observed time for reaction completion was three days for both of them instead of 20 hours.

2.4 Results and Discussion

The first batch of five NMR scale reactions (batch 1) examined the effectiveness of the condensation reaction in solvent mixtures of acetonitrile, DMSO-d₆, plus a third solvent. The DMSO was required to dissolve the BTAC but was usually kept at a minimum as it is often difficult to precipitate the products from solvents containing a lot of DMSO. Experiment C was the exception, as we sought to see if a 50% DMSO: MeCN solvent would favor the reaction. For batch 2 deuterated acetonitrile was used to make the stock [(phen)₂Ru(phendione)][PF₆]₂ solution, as it is commonly used as the solvent of choice for our NMR studies and therefore we have most of our NMR data in this solvent. The third solvent explored was either ethanol (a protic solvent) or glacial acetic acid (weak acid solvent). Two bases were examined, K₂CO₃ and NaOAc. Experiment A examined the effect of not adding any base.

The ^1H NMR spectra for experiments A-E (batch 1) are shown in Figure 2-7. The spectra for A, B, and C experiments are similar to what we had seen previously and showed no signs of the desired product, but instead gave broadened, messy peaks in the aromatic region. Experiment D conducted with ethanol and NaOAc base gave the spectrum of the $[(\text{phen})_2\text{Ru}(\text{phendione})][\text{PF}_6]_2$ starting material, indication of no reaction occurred here at all. Experiment E, however, showed promise as the peaks at 9.6 ppm are characteristic of the tatpp ligand being formed. It also appeared that some $[(\text{phen})_2\text{Ru}(\text{phendione})][\text{PF}_6]_2$ was remaining, indicating an incomplete reaction. Allowing this mixture to react for another 24 h at room temperature, however, did nothing to improve the situation. Even heating to 50°C did nothing to further drive the reaction.

From this initial set of experiments, it was clear that the presence of acetic acid was important for the reaction and that K_2CO_3 seems to be a good base for this reaction. It is recognized that under these reaction conditions, K_2CO_3 is rapidly converted to two equivalents of KOAc, H_2O , and CO_2 .

A second batch of NMR scale experiments was then conducted in which we varied the $[(\text{phen})_2\text{Ru}(\text{phendione})][\text{PF}_6]_2$ to BTAC ratio from 2.2:1 to 2:1, 1.8:1, 1.6: and 1.4:1, under the conditions in Experiment E (MeCN:DMSO:HOAc: K_2CO_3). The ^1H proton NMR spectra for batch 2 showed that experiment J with excess BTAC (having a $[(\text{phen})_2\text{Ru}(\text{phendione})][\text{PF}_6]_2$ to BTAC ratio 1.4:1) did better at going to completion (figure 2-8). For the experiments F-I, the ^1H proton NMR spectra showed extra peaks which is due to remaining unreacted $[(\text{phen})_2\text{Ru}(\text{phendione})][\text{PF}_6]_2$. We assume that the technical grade BTAC has sufficient impurities to warrant the excess of BTAC. Fortunately these impurities do not seem to effect the reaction otherwise. Experiment K showed that the reaction is not very sensitive to the amount of base added, and

experiment L showed that the acetonitrile could not be substituted with DMSO (figure 2-8).

We next tried to scale the reaction using 100 mg of $[(\text{phen})_2\text{Ru}(\text{phendione})][\text{PF}_6]_2$. Here even more BTAC (1.2:1 molar ratio) was required to drive the reaction to completion. It was possible to follow the reaction by taking an aliquot from the reaction solution and removing the MeCN under reduced pressure and then adding CD_3CN to obtain a NMR spectrum. In general, reactions not complete within 20 h require addition of more BTAC to drive the reaction to completion.

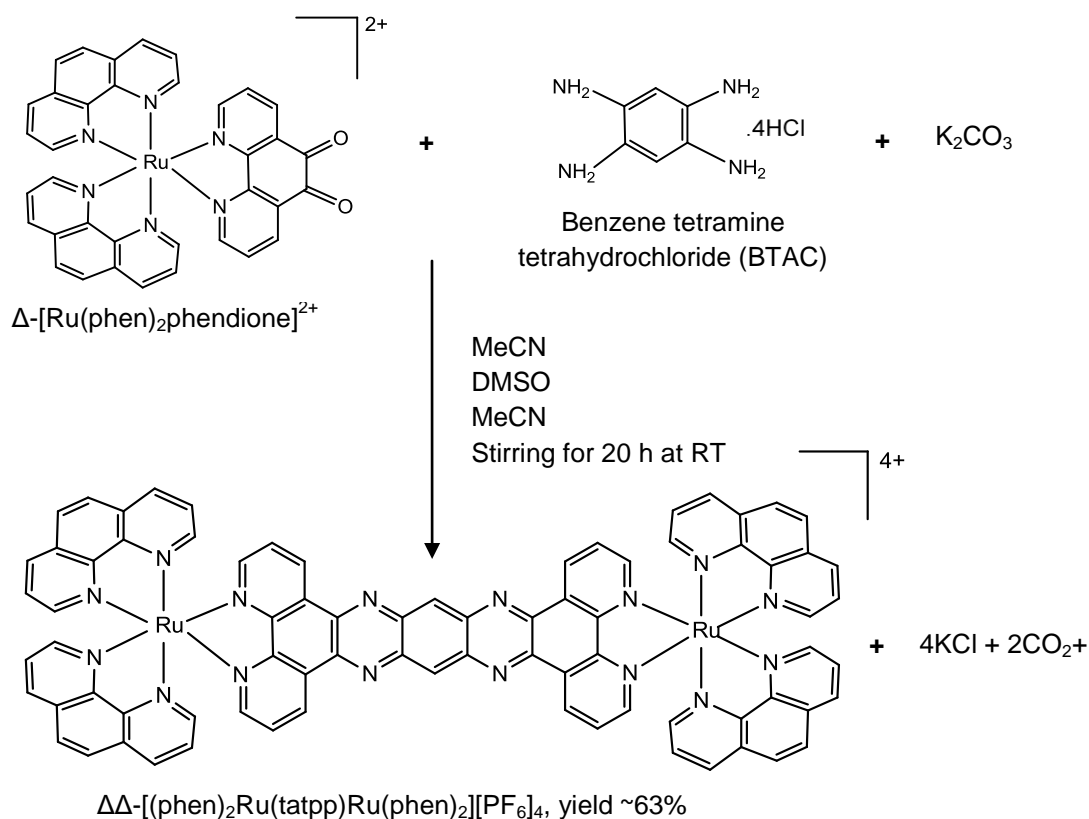


Figure 2-5 New simplified one-step synthesis scheme for enantiopure 4^{4+}

Lastly, we investigated the role of heat on the coupling reaction. Reactions conducted under optimum coupling conditions and stoichiometry but heated either to ~50° C or reflux did not yield clean product, as seen in figure 2-9. While the reaction was sped up, the appearance of side-products suggests heat should be avoided.

In summary, it is possible to now directly prepare $[(\text{phen})_2\text{Ru}(\text{tatpp})\text{Ru}(\text{phen})_2][\text{PF}_6]_4$ from $[(\text{phen})_2\text{Ru}(\text{phendione})][\text{PF}_6]_2$ and BTAC in either enantiopure form as $\Delta\Delta$ or $\Lambda\Lambda$ or as a diastereotopic mixture, depending on the choice of starting material. This synthesis is far more efficient than the previous multi-step procedure and could, in theory, be scaled up substantially.

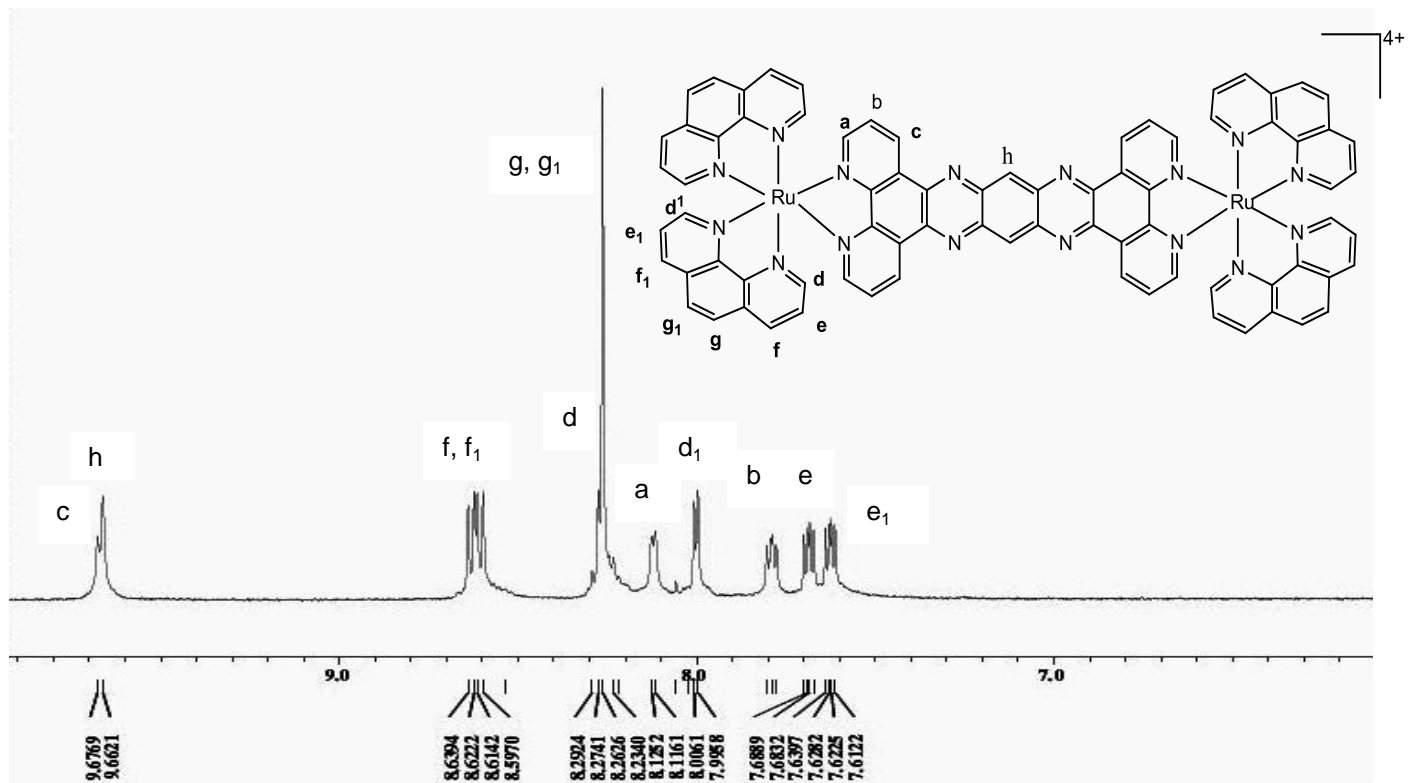


Figure 2-6 ^1H spectra of $[(\text{phen})_2\text{Ru}(\text{tatpp})\text{Ru}(\text{phen})_2][\text{PF}_6]_4$ in CD_3CN

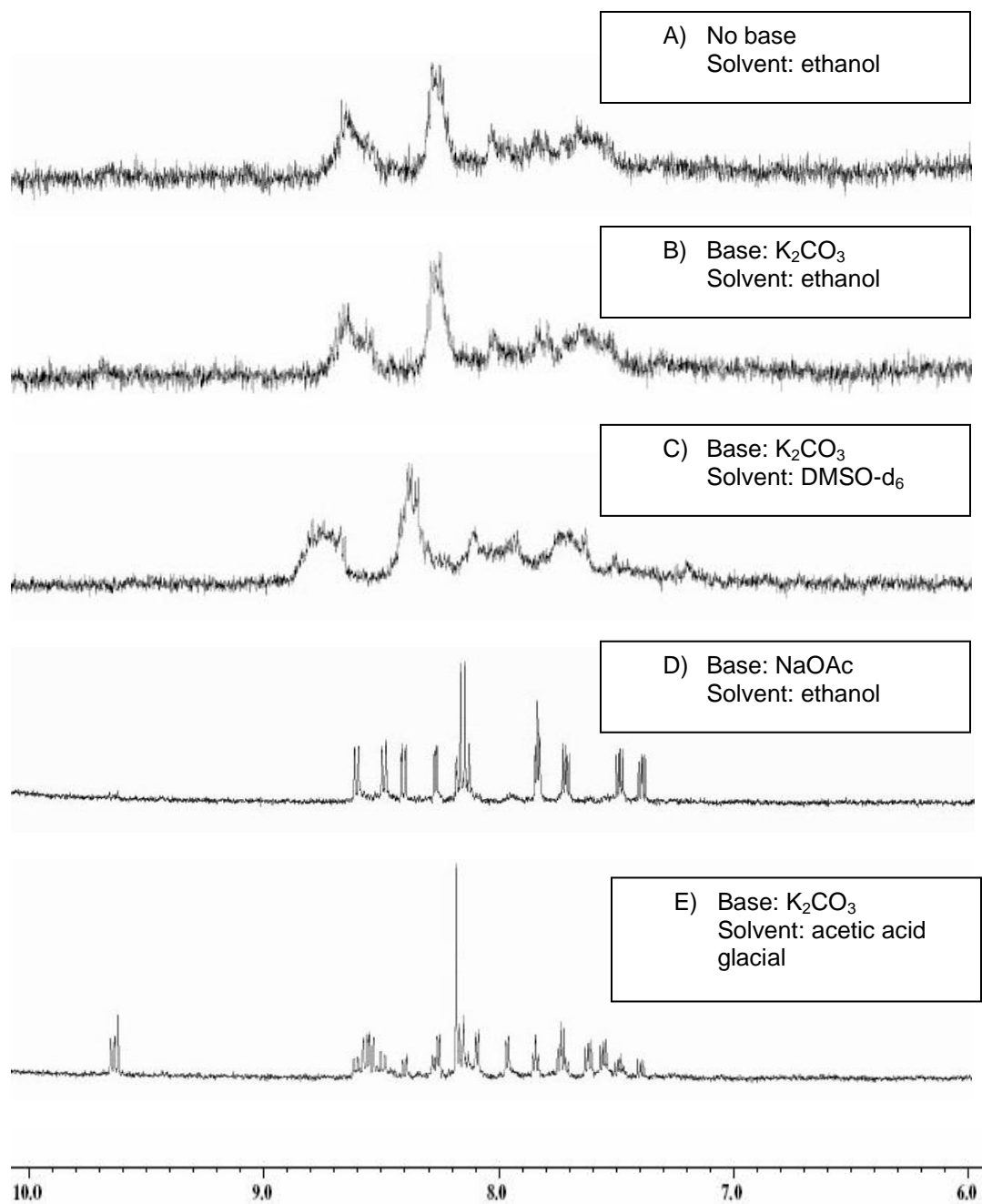


Figure 2-7 1H NMR spectra in $DMSO-d_6$ for NMR scale reactions of batch 1. For all of them molar ratio for $[(phen)_2Ru(phenidone)][PF_6]_2$: BTAC = 2:1. The amount of base used were ~ 15 mg

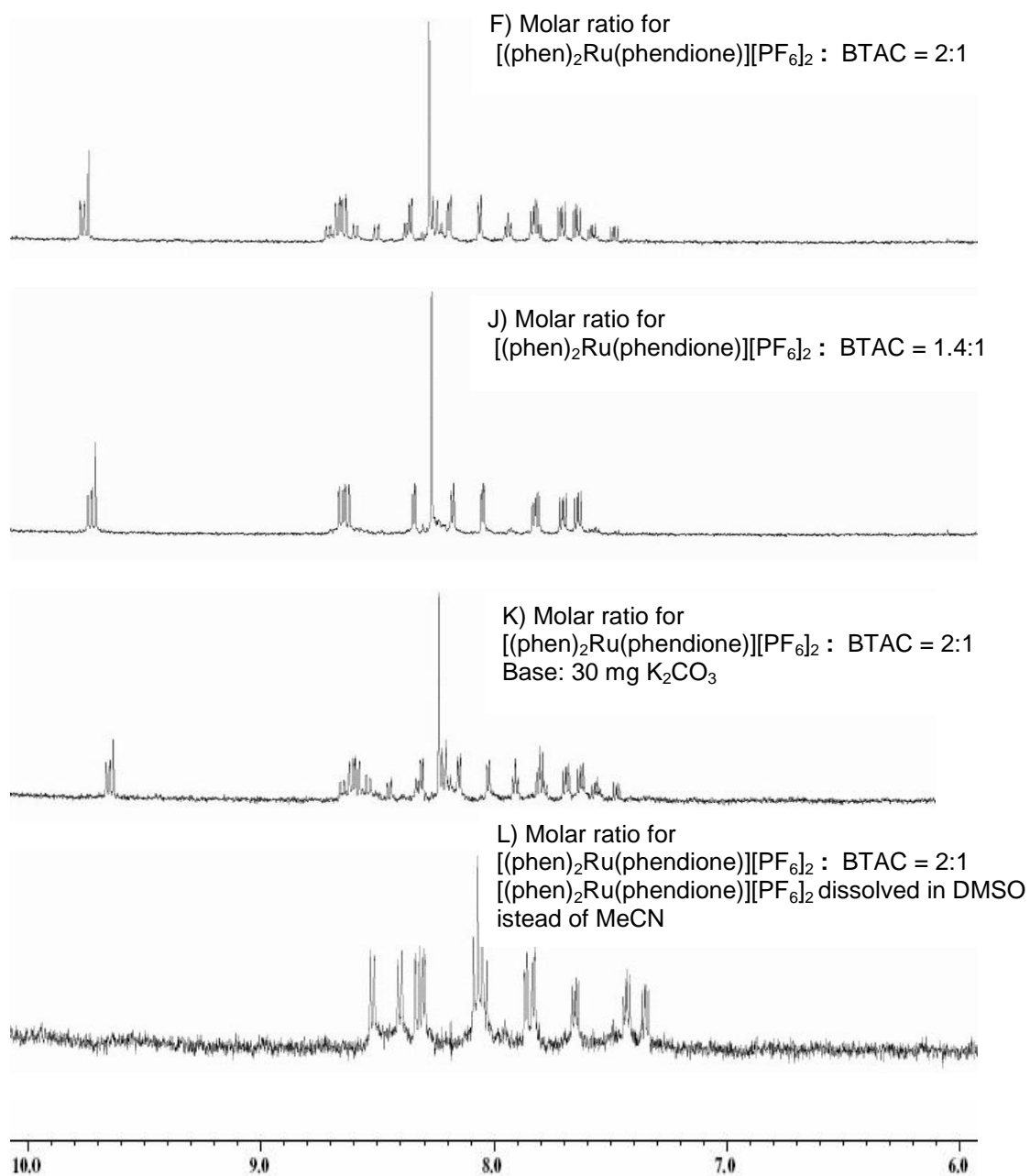


Figure 2-8 ^1H NMR spectra in CD_3CN (tube F, J, K) and DMSO-d_6 (tube L) of NMR scale reactions of batch 2. The amount of base used were ~ 15 mg except K.

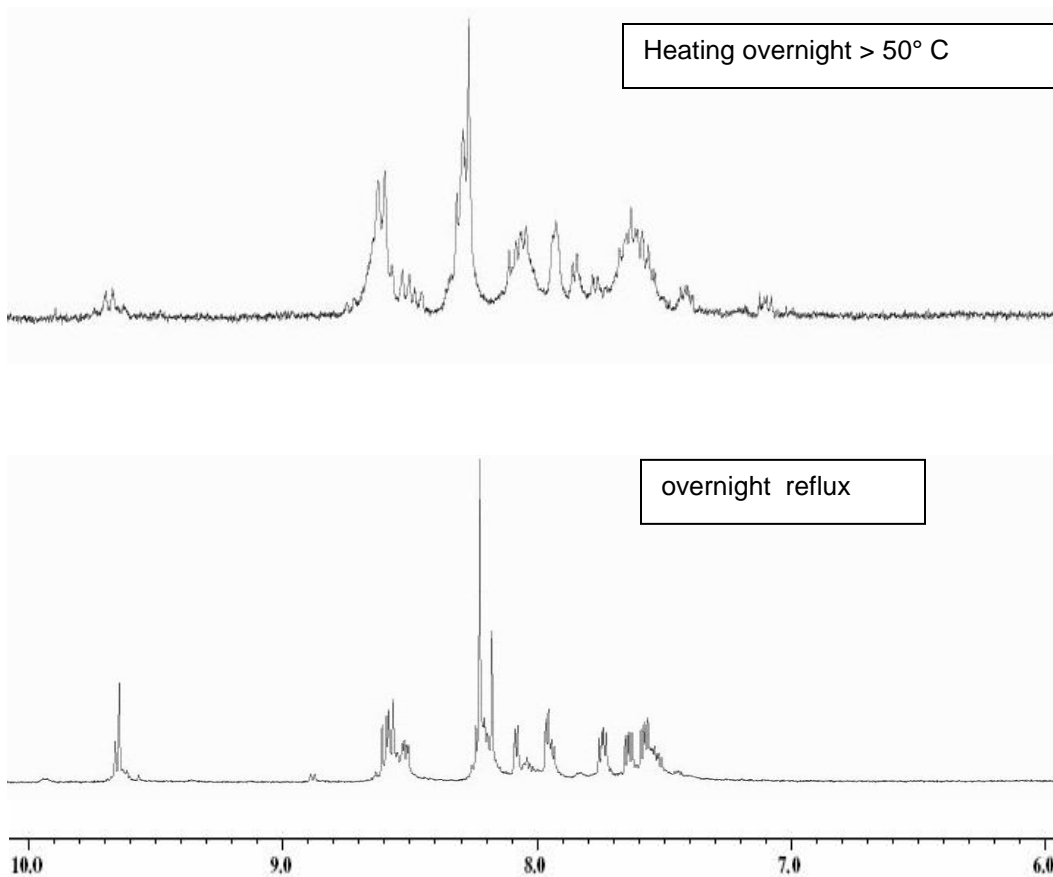


Figure 2-9 ^1H NMR spectra in CD_3CN for the products obtained after overnight reflux and heating via new synthesis approach of $\Delta\Delta\text{-}[(\text{phen})_2\text{Ru}(\text{tatpp})\text{Ru}(\text{phen})_2][\text{PF}_6]_4$

Chapter 3

Effects of Stereochemistry in DNA Photocleavage

3.1 Photodynamic Therapy (PDT) and Photochemotherapeutics (PCT)

Photodynamic therapy (PDT) is based on the concept that the administration of a non-toxic drug (photosensitizer) either systematically or locally can be therapeutic when light is used to photoactivate the drug to become cytotoxic in or near tumor cells.⁴⁶ This therapy can be very efficient at targeting cancer cells and thus limiting damage to non-irradiated tissue.⁹ PDT has been recommended as a treatment option for stage 0 and stage I centrally located early-stage lung cancer by the US National Cancer Institute.⁴⁷

Many PDT agents work by activating O_2 to form any number of reactive oxygen species (ROS) in the close proximity to the tumor cells. There are two principal ROS mechanisms for PDT to work: 1. Reduction of the O_2 to form radical ions and ultimately OH^\cdot and 2. Energy transfer in which singlet oxygen (1O_2) is formed (figure 3-2).⁴⁸ Most PDTs are reported to function via the singlet oxygen route.⁴⁹

3.2 Photo-activation of RPCs Influencing Biological Activity

Most of the PCT agents that are clinically approved to be used in PDT are organic in nature and efficiently produce singlet oxygen. However, transition metal based complexes are also capable of inducing photo-induced DNA damage or cell death by a number of mechanisms in addition to the production of singlet oxygen.²⁶ Due to their favorable photophysical properties, RPCs show considerable promise as PDT agents. The groups of Turro, McFarland, and Glazer have all reported on the use of RPC as photosensitizers for DNA cleavage and for cytotoxicity in cultured malignant cell lines.^{26,31,28} Several classes of RPCs have been identified as being potent photocleavage

agents with visible light (>400 nm) and remain inert in dark. In malignant cell lines, there was a remarkable change in phototoxicity index, (PI) which is the ratio of IC₅₀ in light to IC₅₀ in dark. Turro group has reported two such compounds (Figure 3-1-a) which showed 280 and 710 fold increases, respectively, in PI values in human cervical adenocarcinoma cell line (HeLa cells) . They propose that in addition to singlet oxygen activation, the ligand exchange reactions allow the RPC to form covalent bonds with DNA.^{26,50} The Glazer group has prepared sterically strained RPCs with longer lived triplet MLCT excited state. Due to distortions in octahedral structure, they show ligand ejection after irradiation and provide a path in which DNA-RPC adducts can be formed by covalent interaction.²⁸

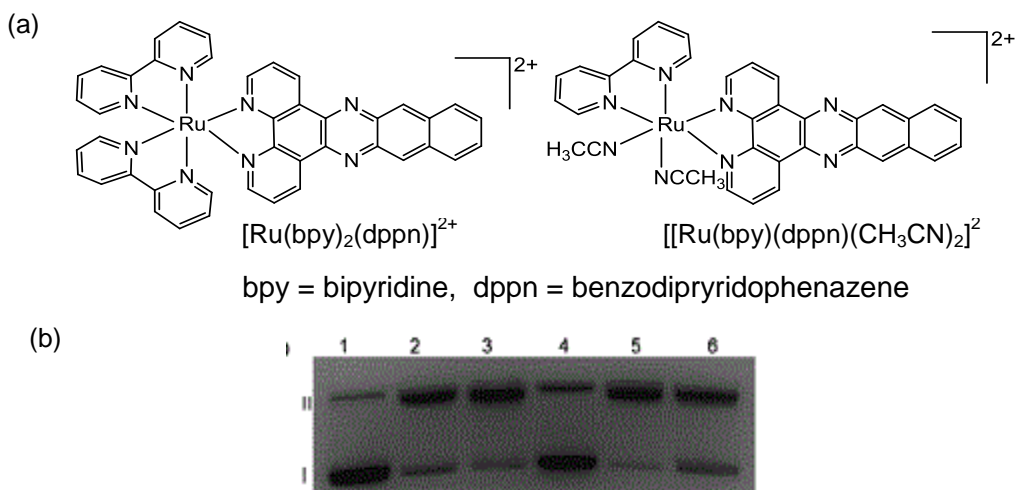


Figure 3-1 (a) Two RPCs tested by Turro group (b) Ethidium bromide stained agarose gels of the photocleavage of 100 μ M pUC18 (5 mM Tris, 50 mM NaCl, pH = 7.5) and 20 μ M of the chloride salt of complex $[Ru(bpy)_2(dppn)]^{2+}$ in air (only except lane 4, ($\lambda_{irr} \geq 475$ nm, $t_{irr} = 50$ seconds), lane 1, dark; lane 2, air; lane 3, D₂O; lane 4, six freeze-pump-thaw cycles (deaerated); lane 5, 2 mM NaN₃ (¹O₂ scavenger); lane 6, 2 units SOD.

The MacDonnell group reported that the RPC, $[(\text{phen})_2\text{Ru}(\text{phendione})]^{2+}$, shows a different mode of photocleavage. Rather than producing ROS, the molecule in its hydrated state abstracts a hydrogen atom from DNA upon visible light irradiation. The active species was assumed to be a metal or carbon-based RPC radical. That radical abstracts a proton from DNA leading to furfural formation. (Figure 3-2)⁵¹

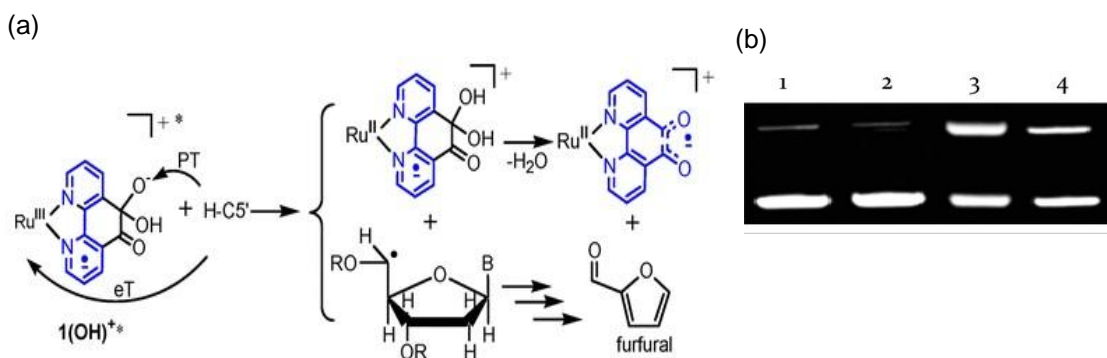


Figure 3-2(a) Photocleavage mechanism of $[(\text{phen})_2\text{Ru}(\text{phendione})]^{2+}$ at physiological pH
 (b) Ethidium bromide stained agarose gels showing photocleavage reactions of 0.154 nM pUC18 DNA bp (4 mM Tris, 50 mM NaCl, pH = 7.4) and 27 μM of the hydrated $[(\text{phen})_2\text{Ru}(\text{phendione})]\text{Cl}_2$, irradiated at 470 nm for 2 h, Lane 1, plasmid; lane 2 in dark and air; lane 3 in irradiation and air; lane 4, irradiation and deaerated

3.3 Previous works regarding DNA photocleavage activity of



RPC $\mathbf{4}^{4+}$ has been found to show promising anti-cancer activity *in vitro* and *in vivo* as a thermal (non-photoactivated complex) agent. In these cases, it appears that the easily reduced tatpp ligand is reductively activated to a doubly reduced state by common cellular reducing agents, such as glutathione (GSH), leading to the efficient production of H_2O_2 from O_2 in the cell nuclei. While this remains an important area of investigation, the photochemistry of $\mathbf{4}^{4+}$ in aqueous solution is well-established and provides another way in which to form reduced tatpp complexes, even in the absence of reducing agents.^{52,53} In these cases, the photoexcited complex is a much more potent oxidant and can be reductively quenched by molecules not typically considered reducing agents, including DNA itself. In an early study of DNA photocleavage by $\mathbf{4}^{4+}$, it was observed that $\mathbf{4}^{4+}$ has an oxygen dependence for cleaving DNA but visible white light (>395nm) does not affect the cleaving potential significantly.⁵⁴

3.4 Experimental

3.4.1 Chemicals

All chemicals required for *in vitro* DNA cleavage assay were purchased commercially and used without any further modification. Autoclaved millipore (18 Ω) water was used to prepare buffer and dissolve $[(\text{phen})_2\text{Ru}(\text{tatpp})\text{Ru}(\text{phen})_2]\text{Cl}_4$ and all the scavengers. Plasmid pUC18 DNA was purchased from Bayou Biolabs. Ethidium bromide from Amresco Inc, EDTA (Ethylenediaminetetraacetic acid) from Alfa Aesar, bromophenol blue from Avacado Research Chemicals, ethanol from Koptech, D-mannitol from Sigma, sodium pyruvate from Mediatech, agarose from Bio Rad, sodium

azide (NaN_3) from Fischer Scientific, trizma base ([tris(hydroxymehtyl)aminomethane]), mono and dibasic phosphate and TEMPO (2,2,6,6-tetramethylpiperidin-1-yl)oxidanyl), were purchased from Sigma Aldrich, respectively. The complex $[(\text{phen})_2\text{Ru}(\text{tatpp})\text{Ru}(\text{phen})_2]_4$ was used as chloride salt.

3.4.2 Buffer preparation

Loading buffer (6X bromophenol blue), 10 mL

25 g bromophenol blue, 6.7 mL of ddH₂O (18 Ω) and 3.3 mL of glycerol was added to a 10 mL glass vial, stirred well and stored at 4°C until use.

0.5 M EDTA (pH 8.0), 1L

148 g of EDTA, ~700 ddH₂O (18 Ω) and sodium hydroxide pellets (~30-40g) were mixed in a 1 L container by stirring. The pH was adjusted to ~8.0 after the EDTA was completely dissolved. Finally, the total volume was made 1 L by adding more ddH₂O (18 Ω).

50X TAE (tris-acetate-EDTA) Stock Solution 1L

242 g Trizma Base was dissolved in ~800 mL of ddH₂O (18 Ω) by stirring in a 1 L container. Next, 57.1 mL Acetic acid glacial and 100 mL of 0.5 M EDTA was added, stirred well and the final volume was made to 1 L by adding ddH₂O (18 Ω).

1X TAE (tris-acetate-EDTA) Running Solution 1L

20 mL of the 50X stock solution was taken in a 1 L container and ~800 mL of ddH₂O (18 Ω) was added and mixed thoroughly. The final volume was made to 1 L and the pH was ~8. The running buffer was kept at room temperature.

50 mM phosphate and 10 mM NaCl buffer at pH 7.4

6 g of sodium phosphate monobasic anhydrous (F.W. 119.98 g/mol), 584 mg of sodium chloride and ~ 800 mL of ddH₂O (18 Ω) was added in a 1 L container and stirred

very well until completely dissolved. The pH was adjusted to 7.4 with concentrated HCl (hydrochloric acid). Once the pH was adjusted, the final volume was made to 1 L and kept at 4°C.

3.4.3 DNA cleavage assay

Plasmid pUC18 DNA was used to conduct DNA cleavage assay via gel electrophoresis at room temperature and in a normoxic condition. 1.2% agarose gel was prepared by staining with ethidium bromide. All the samples were prepared in 1.5 mL centrifuge tubes each having 4 μ L of plasmid DNA (0.154 mM of DNA base pairs) and 8 μ L of 4^{4+} solution (0.0128 mM) prepared in autoclaved ddH₂O (18 Ω). The final volume was raised to 40 μ L by adding 50 mM phosphate buffer (autoclaved, pH 7.4). The order of addition was: buffers at the starting, then 4^{4+} and DNA at the end. In case of using scavengers, the concentrations were maintained as mentioned in figure legends. After addition of DNA and all other chemicals, the tube was vortexed well and spun to make a homogenous mixture. To induce DNA photocleavage, a 470 nm blue light was used. The lamp used to irradiate the samples had one hundred twenty, 470 nm LEDs that are 5 mm in diameter. They were connected in 24 parallel circuits consisting of 5 LEDs/circuit. The samples were transferred to small transparent glass culture tubes for light irradiation. Finally, the culture tubes were placed in a glass beaker which can perfectly fit the inner compartment of the lamp. After the irradiation was done for the designed period of time, the samples were again transferred to the eppendorf tubes before running gel electrophoresis. The samples not subjected to irradiation were prepared in low light. Finally, all the samples prepared for gel electrophoresis were placed in dry ice and acetone to quench plasmid reactions after respective incubation times. The agarose gels

were immersed in TAE buffer and each well received 10 μ L of the samples. The electrophoresis was run for 60 - 70 minutes at 70V.

3.4.4 Instrumentation for analyzing DNA cleavage %

At the end of gel electrophoresis, each gel was imaged in Bio Rad Gel Doc™ XR+ and analyzed in Image Lab software (version 4.1) which gave the % of circular and supercoiled DNA in each band according to densitometry.

3.5 Results and Discussion

The DNA cleavage activity of the complex 4^{4+} has already been proved without light irradiation in both agarose gel electrophoresis assay and in cultured malignant cell lines.^{1,2,3} The electrophoresis assay revealed single strand break (SSB) and only the relaxed circular (OC or form II) and supercoiled (SC or form I) forms appeared in the ethidium bromide stained agarose gels. The double strand break (DSB) was proved via ATM pathway response and γ H2AX double strand break assay. The other two important aspects regarding this 4^{4+} are that, the cleavage is a non-hydrolytic irreversible cleavage which oxidizes the DNA leading to irreversible damage and cell death in presence of a reducing agent glutathione (GSH).^{1,55}

Unlike many metal based bioactive complexes, 4^{4+} can cleave DNA without light irradiation and the cleavage gets more pronounced in low oxygen concentration which is more similar to the environment inside the cancer cells. The MacDonnell's lab has recently reported that the DNA cleavage is more pronounced in high [GSH] / [O₂] (Figure 3-5) due to enhanced H₂O₂ formation over superoxide formation under these conditions. H₂O₂ is far more persistent and toxic than superoxide. This data suggested that the cleavage % is dependent on [GSH] / [O₂] in absence of light irradiation (Figure 3-3).¹

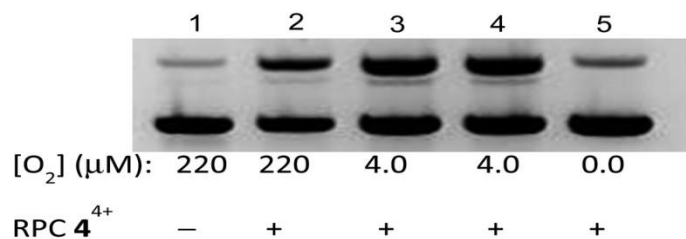


Figure 3-3 *In vitro* DNA plasmid cleavage assay in which pUC19 DNA (154 μM DNA-bp) was incubated with 4⁴⁺ (31 μM) in PBS buffer (pH 7.2) and 1.0 mM GSH at varying [O₂]. Lane 1: control, no 4⁴⁺, 220 mM O₂. Lane 2–5: DNA, 4⁴⁺, and varying amounts of O₂. Lane 4 also contains 30 μM 3,4-dihydroxybenzoate to show that this does not interfere with the assay; lane 5 contains 30 μM 3,4-dihydroxybenzoate and 5 units of protocatechuic dioxygenase

According to the literature, irradiation with white light (>365 nm) did not cause any cleavage under aerobic condition unless reducing agent GSH was added. In an anaerobic environment, prominent photocleavage was only seen in presence of GSH but without GSH the cleavage was insignificant.⁵⁴

3.5.1. Photocleavage of 4⁴⁺ and effects of stereochemistry

Even though 4⁴⁺ does not need photo-activation to exhibit cleavage, we found it necessary to investigate whether 4⁴⁺ is capable of showing increased photocleavage activity after irradiating with more intense LED sources. This time we were also interested to see if the molecule 4⁴⁺ can be activated only by irradiation with visible light and whether GSH is necessary to induce DNA photocleavage. Our hypothesis was that, with the visible light irradiation from more intense LED sources might be able to show increased cleavage because the previous white light irradiation was not enough intense to cause long lived excited state for 4⁴⁺.

Also, as the ΔΔ-form has been proved to be a better candidate to show selective cytotoxicity towards malignant cell-lines, we assumed there might be an effect of

stereochemistry in photocleavage reactions too. We performed plasmid cleavage assay to confirm our hypothesis and observed that the rate of photocleavage is influenced by stereochemistry.

First, two sets of experiments were conducted (with and without GSH) by irradiating plasmid pUC18 DNA with 4^{4+} under 470 nm blue light for 4 hours and 1 hour. The one hour irradiation experiments showed significant cleavage for $\Delta\Delta$ -form and mix- 4^{4+} but a relatively lower cleavage amount for the $\Lambda\Lambda$ -form in absence of GSH. (Figure 3-4). The four hour irradiation experiments caused complete cleavage of supercoiled form both in presence and absence of GSH (Figure 3-5) indicating irradiation time is proportional to photocleavage.

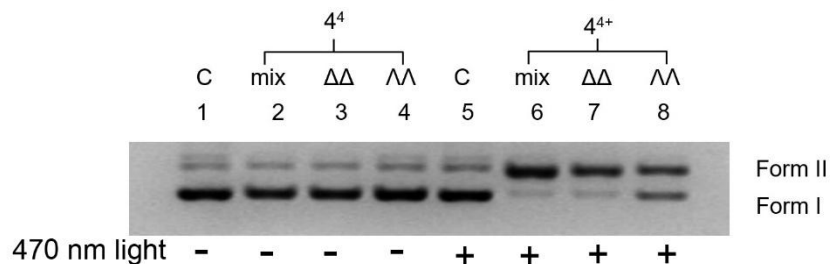


Figure 3-4 Figure 2-3 Agarose gel (1.2%) stained with ethidium bromide showing DNA cleavage product of plasmid pUC18 DNA (0.154 mM DNA-bp) after treatment with 0.0128 mM RPC (mix- 4^{4+} , $\Delta\Delta$ - 4^{4+} and $\Lambda\Lambda$ - 4^{4+}). All the lanes having “-” annotation were incubated in dark for 1 h and all the lanes with “+” annotation were incubated in 470 nm blue light for 1h. (a) Lane 1 control, C; lane 2-4, treated with RPC in dark; lane 5, DNA in light; lane 6-8, treated with RPC in light, Form II shows nicked circular and form I shows supercoiled plasmid DNA

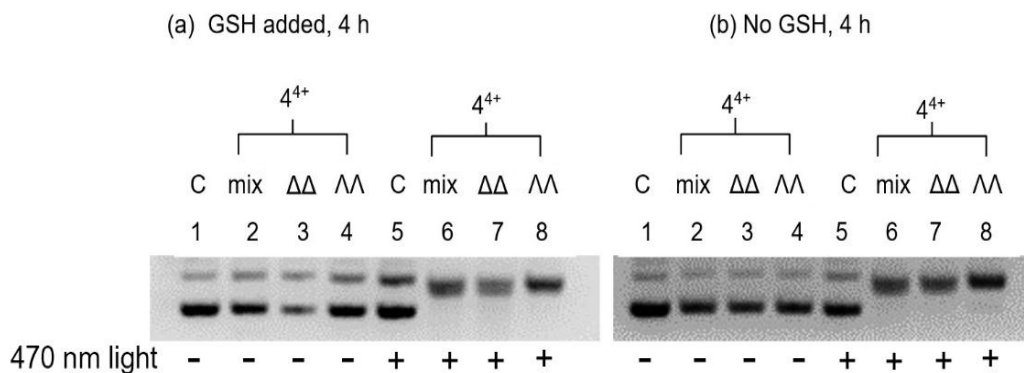


Figure 3-5 Figure 2-3 Agarose gel (1.2%) stained with ethidium bromide showing DNA cleavage product of plasmid pUC18 DNA (0.154 mM DNA-bp) after treatment with 0.0128 mM RPC (mix- 4^{4+} , $\Delta\Delta$ - 4^{4+} and $\Lambda\Lambda$ - 4^{4+}). All the lanes having "-" annotation were incubated in dark for 4 h and all the lanes with "+" annotation were incubated in 470 nm blue light for 4 h. (a) Lane 1 control, C; lane 2-4, treated with RPC and GSH (0.128 mM) in dark; lane 5, DNA in light; lane 6-8, treated with RPC and GSH (0.128 mM) in light (b) Lane 1 control, C; lane 2-4, treated with RPC in dark; lane 5, DNA in light; lane 6-8, treated with RPC in light, Form II shows nicked circular (upper bands) and form I shows supercoiled (lower bands) plasmid DNA

Finally, plasmid cleavage experiments were done with an irradiation time of 30 minutes without adding GSH to demonstrate whether mix- 4^{4+} , $\Delta\Delta$ - 4^{4+} and $\Lambda\Lambda$ - 4^{4+} show any variation in activity with time (Figure 3-6).

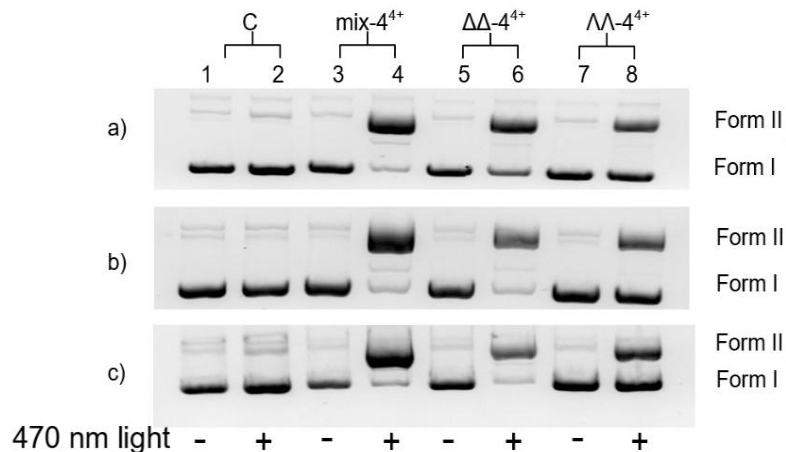


Figure 3-6 Agarose gel (1.2%) stained with ethidium bromide showing DNA cleavage product of plasmid pUC18 DNA (0.154 mM DNA-bp) after treatment with 0.0128 mM RPC (mix-4⁴⁺, ΔΔ-4⁴⁺ and ΛΛ-4⁴⁺). All the lanes having “-” annotation was incubated in dark for 30 min and all the lanes with “+” annotation was incubated in 470 nm blue light for 30 min. Lane 1 and 2 showing control, C and lane 3-8 were treated with RPC. Form II shows nicked circular and form I shows supercoiled plasmid DNA. Form II shows nicked circular and form I shows supercoiled plasmid DNA Images a, b, and c represents same cleavage assay to ensure reproducible results.

The gel images from 30 min irradiation were analyzed to get cleavage % via densitometry. It was found that the mix-4⁴⁺ and ΔΔ-4⁴⁺ caused ~65% and ~57% cleavage respectively whereas ΛΛ-4⁴⁺ only cause ~33% cleavage. The same assay was conducted three times and the results are shown in Table 3-1. The final cleavage % was adjusted with the correction factor 1.4 for supercoiled form I (Figure 3-7) due to its decreased binding to ethidium bromide compared to the relaxed circular form.⁵⁸

Table 3-1 Cleavage % for mix-4⁴⁺, ΔΔ-4⁴⁺ and ΛΛ-4⁴⁺ after 30 min (without correction factor)

		Control		mix-4 ⁴⁺		ΔΔ-4 ⁴⁺		ΛΛ-4 ⁴⁺	
470 nm light		-	+	-	+	-	+	-	+
Run 1	Circular %	5	9	0	91	5	85	5	40
	Supercoiled %	95	91	100	9	95	15	95	60
Run 2	Circular %	4	7	5	90	5	72	5	49
	Supercoiled %	96	93	95	10	95	28	95	51
Run 3	Circular %	4	4	2	89	3	84	3	48
	Supercoiled %	96	96	98	9	97	16	97	52

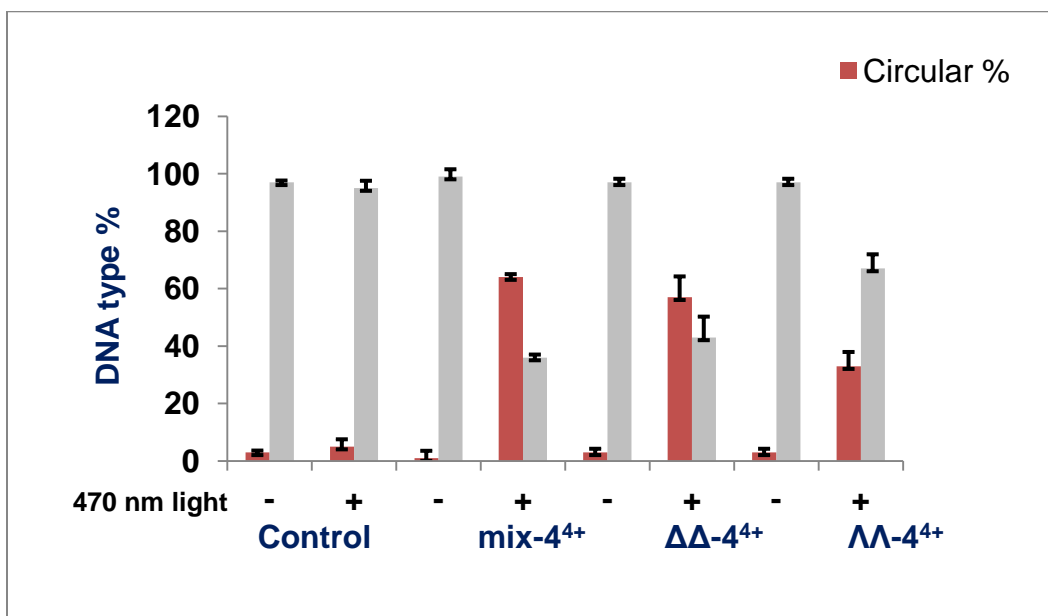


Figure 3-7 Average cleavage % (after applying correction factor 1.4 for circular pUC18 DNA/supercoiled pUC18 DNA) and standard deviation for mix-4⁴⁺, ΔΔ-4⁴⁺ and ΛΛ-4⁴⁺ after 30 min irradiation in 470 nm blue light. The sign “+” was used for irradiation and “-” was used for dark

3.5.2 Active radical species responsible for photocleavage

The next set of experiments was designed to determine the active radical species responsible for this photocleavage reaction. The known photosensitizers cleave DNA via formation of reactive oxygen species (ROS). However, there is another type of radical formation where the photosensitizer itself becomes a radical ion and abstracts a proton from DNA leading to cleavage. This has been reported for a RPC named Δ -[Ru(phen)₂(phendione)]²⁺ in hydrated state at physiological pH where it became carbon centered radical.⁵¹ Kashinge and co-workers showed a good example for carbon centered radicals and their ability to cleave DNA where they used dihydropyrazines.⁵⁶

For the current project, different radical scavengers were used to see quenching in cleaving activity. Mannitol, ethanol and sodium pyruvate were used which are well-known OH[•] scavengers.¹ As singlet oxygen scavenger⁵¹, sodium azide (NaN₃)⁵¹ was chosen and as a carbon or metal based radical scavenger, TEMPO^{51,57} was used. All results are presented in Figure 3-8.

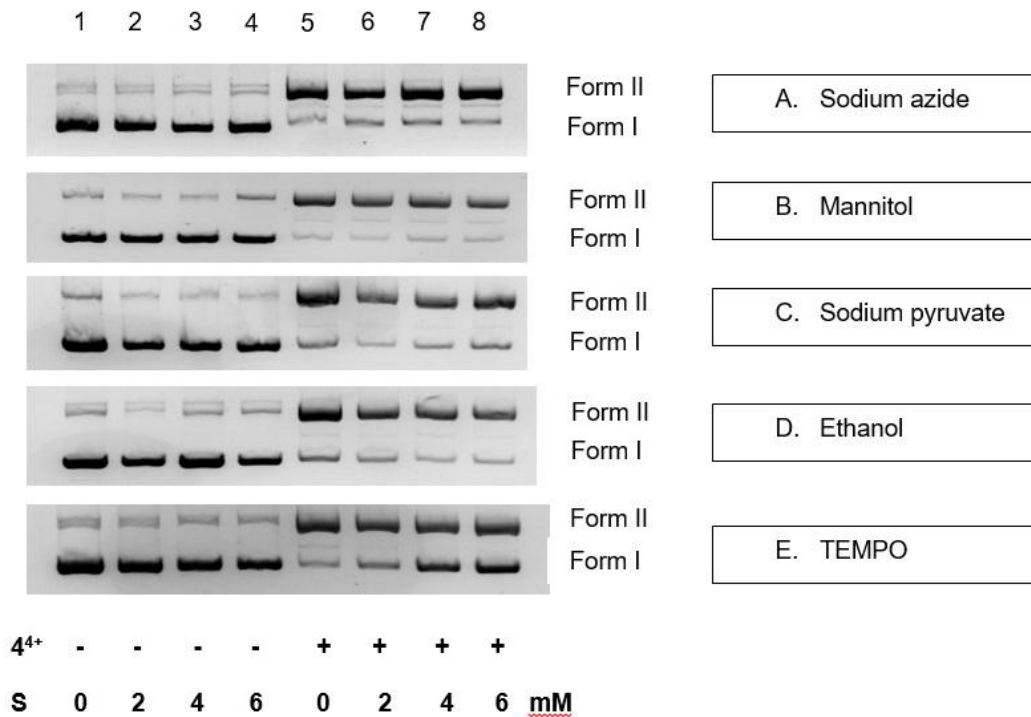


Figure 3-8 Agarose gel (1.2%) stained with ethidium bromide showing DNA cleavage product of plasmid pUC18 DNA (0.154 mM DNA-bp) after irradiating in 470 nm blue light for 30 min. Lane 1-4 do not have any mix-4⁴⁺ and lane 5-8 were treated with mix-4⁴⁺ (0.0128 mM). Images A (sodium azide), B (mannitol), C (sodium pyruvate), D (ethanol) and E (TEMPO) have scavengers added in 0, 2, 4 and 6 mM in lanes 1-4 and 0, 2, 4 and 6 mM in lanes 5-8, respectively. Form II shows nicked circular and form I shows supercoiled plasmid DNA. S represents scavenger

It was clearly evident from Figure 3-8, that scavenger TEMPO can only cause significant quenching of the DNA cleavage reaction mediated by mix-4⁴⁺. Sodium azide gives little effect but ethanol, mannitol and sodium pyruvate caused negligible or no change in cleavage reaction. The densitometry cleavage analysis of these images were performed and found that TEMPO cause reduction in the % cleavage from 61% to 34%. All results are summarized in Table 3-2 and Figure 3-10.

. TEMPO, a known carbon or metal radical scavenger, attenuates the photocleavage activity of 4^{4+} . At present it is hard to put this into a complete cleavage mechanism, but it seems likely that the photoexcited $^3\text{MLCT}$ state with a transient Ru(III) center is reductively quenched by TEMPO. In the absence of TEMPO, this Ru(III) center oxidizes DNA in a manner leading to strand scission. Ruthenium (II) polypyridyl complexes with intercalating ligands like tatpp can undergo electron transfer reaction with DNA. That electron transfer reaction ultimately causes oxidation of DNA bases especially DNA and photo-adduct formation which causes DNA sugar-phosphate backbone cleavage in the end.⁵⁹ Guanine has been identified as the most easily oxidized DNA base.⁵⁸ Also, The highly oxidizing triplet MLCT excited state can directly abstract a hydrogen atom from the sugar-phosphate backbone of DNA leading to DNA strand break. Definitive proof of DNA photooxidation would be to isolate and detect the photo-adduct or presence of furfural or 5-MF in the cleavage products. Furfural or 5-MF is the result of hydrogen atom abstraction from DNA sugar.^{51,59} These experiments have not been done yet for the complex 4^{4+} , but are proposed (fig 3-9).

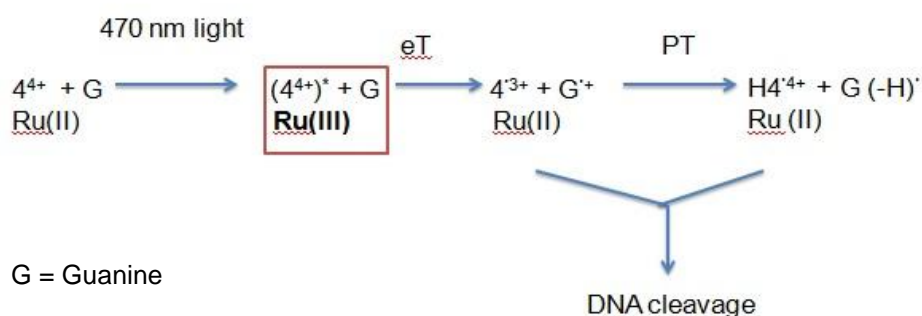


Figure 3-9 Electron transfer between 4^{4+} and DNA leading to DNA-base oxidation and photo-cleavage

Table 3-2 DNA cleavage reaction results of mix-4⁴⁺ with various radical scavengers detected by densitometry

mix-4 ⁴⁺ (.00128 mM)	-		-	-	-	+	+	+	+	+
Scavenger conc. (mM)			0	2	4	6	0	2	4	6
NaN ₃	Form II		0	6	4	4	62	54	58	60
	Form I		100	94	96	96	38	46	42	40
Mannitol	Form II		9	6	6	12	64	71	69	64
	Form I		91	94	94	88	36	29	31	36
pyruvate	Form II		9	6	7	6	58	60	60	57
	Form I		91	94	93	94	42	40	40	43
ethanol	Form II		9	0	6	11	54	53	59	58
	Form I		91	100	94	89	46	47	41	42
TEMPO	Form II		6	6	7	8	61	52	36	34
	Form I		94	94	93	92	39	48	64	66

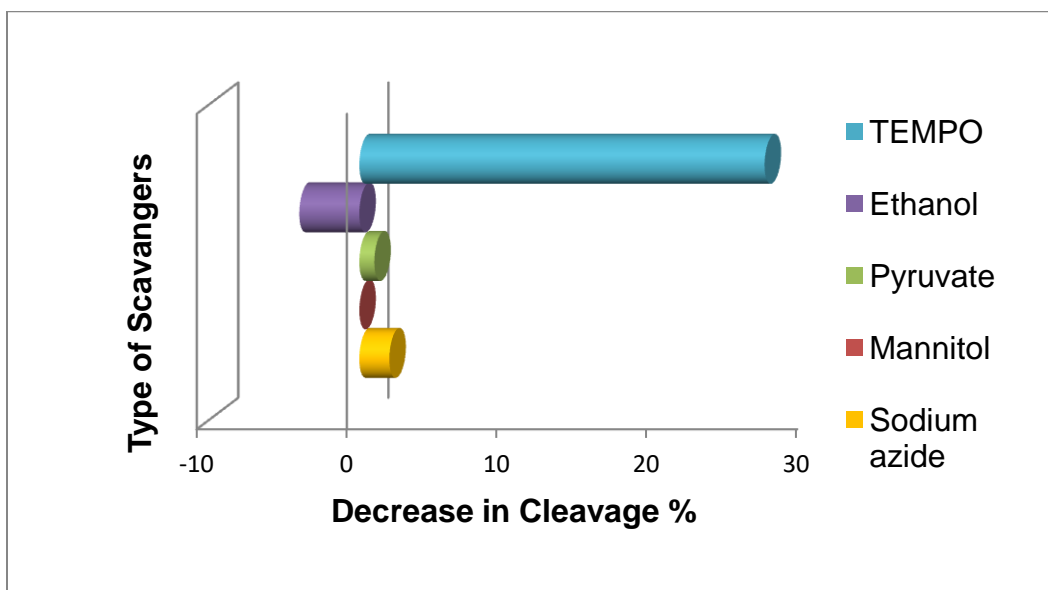


Figure 3-10 decrease in DNA photocleavage activity after addition of scavengers

TEMPO was found to have remarkable cleavage quenching ability, we performed another set of plasmid cleavage assay with $\Delta\Delta-4^{4+}$ and $\Lambda\Lambda-4^{4+}$ to see whether the TEMPO mediated quenching effect was also present for them. For both of them a remarkable decrease in photocleavage activity was observed after Addition of TEMPO ($\Delta\Delta-4^{4+}$ reduced from 49% cleavage to 36% cleavage and $\Lambda\Lambda-4^{4+}$ reduced from 32% cleavage to 13% cleavage of supercoiled plasmid DNA) (Figure 3-11)

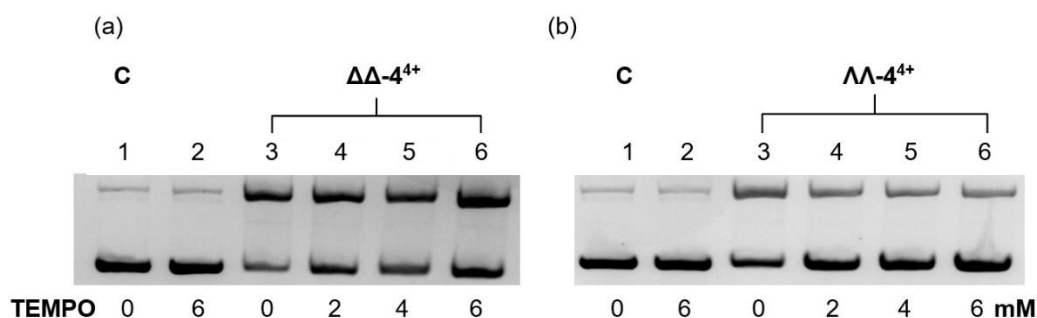


Figure 3-11 Agarose gel (1.2%) stained with ethidium bromide showing DNA cleavage product of plasmid pUC18 DNA (0.154 mM DNA-bp) after irradiating in 470 nm blue light for 30 min. (a) Lane 1, control; lane 2, 6 mM TEMPO; lane 3, 0.0128 mM $\Delta\Delta-4^{4+}$; lane 4-6, 0.0128 mM $\Delta\Delta-4^{4+}$, 6 mM TEMPO (b) Lane 1, control; lane 2, 6 mM TEMPO; lane 3, 0.0128 mM $\Lambda\Lambda-4^{4+}$; lane 4-6, 0.0128 mM $\Lambda\Lambda-4^{4+}$, 6 mM TEMPO.

Form II shows nicked circular (upper bands) and form I (lower bands) shows supercoiled plasmid DNA

3.6 Conclusion

According to the gel electrophoresis experiments after irradiation, $\Delta\Delta-4^{4+}$ appears to be more active than $\Lambda\Lambda-4^{4+}$ as it shows greater cleavage in short irradiation periods but both $\Delta\Delta-$ and $\Lambda\Lambda$ forms bind to DNA and cause DNA photocleavage. At longer irradiation periods, both give 100% photocleavage. The cleavage mechanism does not require an external reducing agent such as GSH, although the presence of such agents leads to even better DNA cleavage. Scavenger experiments with alcohols and sugars

showed no effect on the photocleavage suggesting that hydroxyl radicals are not involved in the cleavage mechanism. Sodium azide also does little to affect the cleavage activity, ruling out singlet O_2 being the causative agent. On the other hand, TEMPO caused quenching of the photocleavage reaction indicating a carbon or metal based radical as the responsible photocleavage or DNA oxidation causing species. Previously, RPCs showing cleavage in such manner was found to cause direct DNA oxidation by abstracting an electron from DNA base guanine. A plausible mechanism for the photocleavage of 4^{4+} involves proton couple electron transfer (PCET) from guanine to the highly oxidizing 3MLCT excited state of 4^{4+} which eventually cause strand scission because the photocleavage activity has been seen mostly for the RPCs having non-chelating nitrogen atoms which can act like a base to accommodate the proton.⁵⁹

References

1. Griffith, C.; Dayoub, A. S; Jaranatne, T.; Alatrash, N.; Mohamedi, A.; Abayan, K.; Bierbach, Z.; Armstrong, D. W.; MacDonnell, F. M. Cellular and cell-free studies of catalytic DNA cleavage by ruthenium polypyridyl complexes containing redox-active intercalating ligands. *Chemical Science*, 2017
2. Alatrash, N.; Narh, E. S.; Yadav, A.; Kim, M. J.; Janaratne, T.; Gabriel, J.; Macdonnell, F. M. Synthesis, DNA cleavage activity, cytotoxicity, acetylcholinesterase inhibition, and acute murine toxicity of redox-Active ruthenium(II) polypyridyl complexes. *ChemMedChem*, 12 (13), 2017, 1055-1069
3. Yadav, A.; Janaratne, T.; Krishnan, A.; Singhal, S. S.; Yadav, S.; Dayoub, A. S.; Hawkins, D. L.; Awasthi, S.; MacDonnell, F. M. Regression of lung cancer by hypoxia sensitizing ruthenium polypyridyl complexes. *Mol Cancer Ther*; 12 (5), 2013, 643 - 653
4. Zeng, L; Gupta, P; Chen, Y; Wang, E; Ji, L; Chao, H; Chen, Z. S. The development of anticancer ruthenium (II) complexes: from single molecule compounds to nanomaterials. *Chem Soc Rev* 2017
5. Killand, L. R. "Of mice and men": values and liabilities of the athymic nude mouse model in anticancer drug development. *European Journal of Cancer* 2004, 40, 827-836.
6. Bratsos, I.; Jedner, S.; Glanferrara , T.; Alessio, E. Ruthenium anticancer compounds: challenges and expectations. *CHIMIA* 61 (2007) 692-697
7. Alderden, A. R.; Hall, M. D.; Hambley, T. W. The discovery and development of cisplatin. *Journal of Chemical Education* (2006), 83(5), 728-734

8. Rijt, S. H. V; Sadler, P. J. Current application and future potential for bioinorganic chemistry in the development of anticancer drugs. *Drug Discovery Today* 2009, 14, 1089-1097
9. Butler, J. S.; Woods, J. A.; Farrer, N. J.; Newton, M. E; Sadler, P. J. Tryptophan switch for a photoactivated platinum anticancer complex. *J. Am. Chem. Soc.* 2012, 134, 16508 – 16511
10. Stordal, B.; Pavlakis, N.; Davey, R. Oxaliplatin for the treatment of cisplatin-resistant cancer: A systematic review. *Cancer Treatment Reviews* (2007) 33, 347 – 357
11. Rajeshwaran, A.; Trojan, A.; Burnand, B.; Giannelli, M. Efficacy and side effects of cisplatin- and carboplatin-based doublet chemotherapeutic regimens versus non-platinum-based doublet chemotherapeutic regimens as first line treatment of metastatic non-small cell lung carcinoma: A systematic review of randomized controlled trials. *Lung Cancer* (2008) 59, 1-11
12. Hartinger, C. G.; Groessl, M.; Meier, S. M.; Casini, A.; Dyson, P. J. Application of mass spectrometric techniques to delineate the modes-of-action of anticancer metallodrugs. *Chem. Soc. Rev.*, 2013, 42, 6186–6199
13. Antonarakis, E. S.; Emadi, A. Ruthenium-based chemotherapeutics: are they ready for prime time? *Cancer Chemother Pharmacol.*, 2010, 66, 1–9
14. Minchinton, A. I.; Tannock, I. F. Drug penetration in solid tumors. *Nat. Rev. Cancer*, 2006, 6, 583–592
15. Trondl, R.; Heffeter, P.; Kowol, C. R.; Jakupec, M. A.; Berger, W.; Keppler, B. K. NKP-1339, the first ruthenium-based anticancer drug on the edge of clinical application. *Chem. Sci.*, 2014, 5, 2925
16. Dwyer, F. P.; Gyarfás, E. C. Biological activity of complex ion. *Nature* 1952, 170 (4318) 190 -191

17. Dwyer, F. P.; Mayhew, E. .; Roe, E. M. F.; Shulman, A. Inhibition of Landschütz ascites tumour growth by metal chelates derived from 3,4,7,8-tetramethyl-1,10-phenanthroline. *Br J Cancer*, 1965, 19, 195-199
18. Koch, J. H.; Rogers, W. P.; Dwyer, F.; P. The metabolic Fate of tris-1, 10-phenanthroline 106 ruthenium (II) perchlorate, a compound with acetylcholinesterase and curare-like activity. *Australian Journal of Biological Sciences* 1957, (10), 342 – 350
19. Tan, C.; Wu, S.; Lai, S.; Wang, M.; Chen, Y.; Zhou, L.; Zhu, Y.; Lian, W.; Peng, W.; Ji, L. Synthesis, structures, cellular uptake and apoptosis-inducing properties of highly cytotoxic ruthenium-Norharman complexes. *Dalton Trans.*, 2011, 40, 8611–8621
20. Cecchin, M. R. Gill.; Walker, M. G.; Mulla, R. S.; Battaglia, G.; Smythe, C.; Thomas, J. A. Targeting the endoplasmic reticulum with a membrane-interactive luminescent ruthenium(II) polypyridyl complex. *Chem. Sci.*, 2013, 4, 4512–4519
21. Satyanarayana, S.; Dabrowaik, J. C.; Chaires, J. B. Thris(phenanthroline)ruthenium (II) enantiomer interactions with DNA: mode and specificity of binding. *Biochemistry* 1993, 32, 2573-2584
22. Zeng, Z.-P.; Wu, Q.; Sun, F.-Y.; Zheng, K.-D.; Mei, W.-J. Imaging nuclei of MDA-MB-231 breast cancer cells by chiral ruthenium(II) complex coordinated by 2-(4-phenylacetylenophenyl)-1H-imidazo[4,5f][1,10]phenanthroline. *Inorg. Chem.*, 2016, 55, 5710–5718
23. Mari, C.; Pierroz, V.; Ferrari, S.; Gasser, G. Combination of Ru (II) complexes and light: new frontiers in cancer therapy. *Chem. Sci.*, 2015, 6, 2660–2686
24. Singh, T. N.; Turro, C. Photoinitiated DNA binding by cis-[Ru(bpy)₂(NH₃)₂]²⁺. *Inorg. Chem.*, 2004, 43, 7260–7262

25. Salassa, L.; Ruiu, T.; Garino, C.; Pizarro, A. M.; Bardelli, F.; Gianolio, D.; Westendorf, A.; Bednarski, P. J.; Lamberti, C.; Gobetto R.; Sadler, P. J. EXAFS, DFT, light-induced nucleobase binding, and cytotoxicity of the photoactive complex $\text{cis-[Ru(bpy)2(CO)Cl]}^+$. *Organometallics*, 2010, 29, 6703–6710
26. Albani, B. A.; Pena, B.; Leed, N. A.; Paula, N. A. B. G. de.; Pavani, C.; Baptista, M. S.; Dunbar, K. R.; Turro, C. Marked improvement in photoinduced cell death by a new tris-heteroleptic complex with dual action: singlet oxygen sensitization and ligand dissociation. *J. Am. Chem. Soc.*, 2014, 136, 17095–17101
27. Glazer, E. C. Light-activated metal complexes that covalently modify DNA. *Isr. J. Chem.*, 2013, 53, 391–400
28. Hidayatullah, A. H.; Watchter, E.; Heidary, D. K.; Parkin, S.; Glazer, E. C. Photoactive Ru (II) complexes with dioxinophenanthroline ligands are potent cytotoxic agents. *Inorg. Chem.* 2014, 53, 10030 – 10032
29. Wachter, E.; Zamora, A.; Heidary, D. K.; Ruiz, J.; Glazer, E. C. Geometry matters: inverse cytotoxic relationship for *cis/trans*-Ru(II) polypyridyl complexes from *cis/trans*- $[\text{PtCl}_2(\text{NH}_3)_2]$. *Chem. Commun.*, 2016, 52, 10121–10124
30. Monro, S.; Scott, J.; Chouai, A.; Lincoln, R.; Zong, R.; Thummel, R. P.; McFarland, S. A. Photobiological Activity of Ru(II) dyads based on (Pyren-1-yl)ethynyl derivatives of 1,10-phenanthroline. *Inorg. Chem.*, 2010, 49, 2889–2900
31. Lincoln, Richard.; Kohler, L.; Monro, S.; Yin, H.; Stephenson, M.; Zong, R.; Chouai, A.; Dorsey, C.; Henninger, R.; Thummel, R.; McFarland, S. A. Exploitation of long Lived ^3IL excited state for metal-organic photodynamic therapy: varification in a Melanoma Model. *J. Am. Chem. Soc.* 2013, 135, 17161 – 17175
32. Stephenson, M.; Reichardt, C.; Pinto, M.; Waächtler, M.; Sainuddin, T.; Yin, G. Shi, H.; Monro, S.; Sampson, E.; Dietzek, B.; McFarland, S. A. Ru(II) dyads derived from

- 2-(1-Pyrenyl)-1H-imidazo[4,5-f][1,10]phenanthroline: versatile photosensitizers for photodynamic applications. *J. Phys. Chem. A*, 2014, 118, 10507–10521
33. Arenas, Y.; Monro, S.; Shi, G.; Mandel, A.; McFarland, S.; Lilge, L. Photodynamic inactivation of *Staphylococcus aureus* and methicillin-resistant *Staphylococcus aureus* with Ru(II)-based type I/type II photosensitizers. *Photodiagn. Photodyn. Ther.*, 2013, 10, 615–625
34. Dayoub, A. Cytotoxicity, Cellular localization and fluorescent microscopy of malignant cells treated with ruthenium (II) complexes of tetraazatetrapyridopentacene ligand. Master of Science, 2015
35. Tuite, E.; Lincoln, P.; Norden, B., Photophysical evidence that δ^- and L-[Ru(phen)₂(dppz)]²⁺ Intercalate DNA from the Minor Groove. *J. Am. Chem. Soc.* 1997, 119 (1), 239-2
36. Norden, B.; Lincoln, P.; Akerman, B.; Tuite, E., DNA interactions with substitution-inert transition metal ion complexes. *Metal ions in biological systems* 1996, 33, 177-252
37. Haq, I.; Lincoln, P.; Suh, D.; Norden, B.; Chowdhry, B. Z.; Chaires, J. B., Interaction of δ^- and L-[Ru(phen)₂DPPZ]²⁺ with DNA: A Calorimetric and equilibrium binding study. *Journal of the American Chemical Society* 1995, 117 (17), 4788-96
38. Le, V. H.; McGuire, R. M.; Ahuja, P.; Macdonnell, F. M.; Lewis, E. A.; Thermodynamic investigations of [(phen)₂Ru(tatpp)Ru(phen)₂][PF₆]₄ interactions with B-DNA. *J. Phys. Chem. B* 2015, 119, 65-71
39. Kim, M.-J.; Thesis, Doctor of Philosophy, University of Texas at Arlington, 2000
40. Yadav, A.; Investigation of redox-active ruthenium(II) polypyridyl complexes as potential anti-cancer drugs. Doctor of Philosophy, University of Texas at Arlington, 2008

41. Chen, Y.; Ruthenium(II) polypyridyl complexes as potential anti-cancer drugs: synthesis, characterization, cell Permeability and localization. Doctor of Philosophy, University of Texas at Arlington, 2013
42. Iger, J.; Gourdon, A.; Ishow, E.; Launay, J. P., Mononuclear and binuclear tetrapyrido[3,2-a:2',3'-c:3'',2''-h:2''',3''''-j]phenazine (tpphz) ruthenium and Osmium complexes. *Inorg. Chem.* 1996, 35 (10), 2937-2944
43. Sullivan, B. P.; Salmon, D. J.; Meyer, T. J., Mixed phosphine 2,2' bipyridine complexes of ruthenium. *Inorg. Chem.* 1978, 17 (12), 3334-3341
44. Hartshorn, R. M.; Barton, J. K., Novel Dipyrido phenazine Complexes of ruthenium(II): exploring luminescent reporters of DNA. *J. Am. Chem. Soc.* 1992, 114 (15), 5919-5925
45. Sun, P.; Krishnan, a.; Yadav, A.; Singh, S.; Macdonnell, F. M.; Armstrong, D. W.; Enantiomeric separations of Ruthenium(II) polypyridyl complexes using high performance liquid chromatography (HPLC) with cyclodextrin chiral stationary phases (CSPs). *Inorg. Chem.* 2007, 46, 10312 – 1032
46. Robertson, C. A.; Evans, H.; Abrahamse, H. Photodynamic therapy (PDT): A short review on cellular mechanisms and cancer research applications for PDT. *Journal of Photochemistry and Photobiology B: Biology* 96 (2009) 1–8
47. Usuda, J.; Kato, H.; Okunaka, T.; Furukawa, K.; Tsutsui, H.; Yamada, K.; Suga, Y.; Honda, H; Ohira, T.; Tsuboi, M.; MD, Hirano, T. Photodynamic therapy (PDT) for lung cancers. 2006, 1 (5), 489-493
48. Jain, R. K.; Fukumura, D.; Dolmans, D.. E. G. J. Photodynamic therapy for cancer. *Nature Reviews Cancer* 3, 380–387 (2003)

49. Josefsen, L. B.; Boyle, R. W. Photodynamic therapy and the development of metal-based photosensitisers. *Metal-Based Drugs*. 2008, Article ID 276109. doi:10.1155/2008/276109
50. Sun, y.; Joyce, L. E.; Dickson, N. M.; Turro, C. Efficient DNA photocleavage by $[\text{Ru}(\text{bpy})_2(\text{dppn})]^{2+}$ with visible light. *Chem. Commun.* 2010, 46, 2426 – 2428
51. Poteet, S. A.; Majewski, M. B.; Breitbatch, Z. S.; Griffith, C. A.; Sing, S.; Armstrong, D. W.; Wolf, M. O.; MacDonnell, F. M. Cleavage of DNA by proton coupled electron transfer to a photoexcited, hydrated Ru (II) 1, 10-phenanthroline-5,6-dione complex. *Am. Chem. Soc.* 2013, 135, 2419-2422
52. Chiroboli, C.; Fracasso, S.; Scandola, F.; Campagna, S.; Serroni, s.; Konduri, R.; Macdonnell, F. M. Primary charge separation in photoinduced multielectron storage systems: A dinuclear ruthenium (II) species featuring a charge-separated state with a lifetime of 1.3 μs . *Chem. Commun.* 2013, 1658 – 1659
53. Tacconi, N. R. D.; Lezna, R. O.; Konduri, R.; Ongeri, F.; Rajeshwar, K.; Macdonnell, F. M. Influence of pH on the photochemical and electrochemical reduction of the dinuclear ruthenium complex, $[(\text{phen})_2\text{Ru}(\text{tatpp})\text{Ru}(\text{phen})_2]\text{Cl}_4$, in water: proton coupled sequential and concerted multi-electron reduction. *Chem. Eur. J.* 2005, 11, 4327 – 4339
54. Ongeri, F. Investigations of the mechanism OF DNA cleavage using Ruthenium polypyridyl complexes. Doctor of Philosophy, University of Texas at Arlington, 2007
55. Griffith, C. Doctor of Philosophy. Towards establishing the mechanism of DNA cleavage by redox-active ruthenium (II) polypyridyl complexes. University of Texas at Arlington, 2015

56. Kashige, N. Y., Tadatoshi; Miake, Fumio; Watanabe, Kenji. Nucleotide sequence Specificity in DNA cleavage caused by dihydropyrazines, a new type of DNA strand-cleaving agent. *Biol.Pharm.Bull.* 2000, 23, 1281-1286
57. Iminyl radicals from arylhydrazones in the photo-induced DNA cleavage. *Bioinorganic and Medicinal Chemistry.* 2004, 12, 2509 – 2515
58. Stemp, E. D. A.; Arkin, M. R.; Barton, J. K. Oxidation of Guanine in DNA by $\text{Ru}(\text{phen})_2(\text{dppz})^{3+}$ Using the Flash-Quench Technique. *J. Am. Chem. Soc.*, 1997, 119 (12), 2921 – 2925
59. Elias, B.; Mesmaeker, K. D. Photo-reduction of polycyclic aromatic Ru (II) complexes by biomolecules and possible applications. *Coordination Chemistry Reviews.* 2006, 250, 1627 – 1641
60. Hartshorn, R. M.; Barton, J. K., Novel Dipyridophenazine Complexes of Ruthenium(II): Exploring Luminescent Reporters of DNA. *J. Am. Chem. Soc.* 1992, 114 (15), 5919-5925